ALS-FUS mutation affects the activities of HuD/ELAVL4 and FMRP leading to axon phenotypes in motoneurons

Maria Giovanna Garone[1], Nicol Birsa[2,3], Maria Rosito[4], Federico Salaris[1,4], Michela Mochi[1], Valeria de Turris[4], Remya R. Nair[5], Thomas J. Cunningham[5], Elizabeth M. C. Fisher[2], Mariangela Morlando[6], Pietro Fratta[2] and Alessandro Rosa[1,4,7,*]

1. Department of Biology and Biotechnology Charles Darwin, Sapienza University of Rome, P.le A. Moro 5, 00185 Rome, Italy
2. UCL Queen Square Institute of Neurology, University College London, London, WC1N 3BG, UK
3. UK Dementia Research Institute, University College London, London, WC1E 6BT, UK
4. Center for Life Nano- & Neuro-Science, Fondazione Istituto Italiano di Tecnologia (IIT), 00161 Rome, Italy
5. MRC Harwell Institute, Oxfordshire, OX11 0RD, UK
6. Department of Pharmaceutical Sciences, "Department of Excellence 2018-2022", University of Perugia, Perugia, Italy.
7. Laboratory Affiliated to Istituto Pasteur Italia-Fondazione Cenci Bolognetti, Department of Biology and Biotechnology Charles Darwin, Sapienza University of Rome, Viale Regina Elena 291, 00161 Rome, Italy

* Corresponding author: alessandro.rosa@uniroma1.it; Tel: +39-0649255218

ABSTRACT

Mutations in the RNA-binding protein (RBPs) FUS have been genetically associated with the motoneuron disease amyotrophic lateral sclerosis (ALS). Using both human induced pluripotent stem cells and mouse models, we found that FUS-ALS causative mutations affect the activity of two relevant RBPs with important roles in neuronal RNA metabolism: HuD/ELAVL4 and FMRP. Mechanistically, mutant FUS leads to upregulation of HuD protein levels through competition with FMRP for *HuD* mRNA 3'UTR binding. In turn, increased HuD levels overly stabilize the transcript levels of its targets, NRN1 and GAP43. As a consequence, mutant FUS motoneurons show increased axon branching and growth upon injury, which could be rescued by dampening NRN1 levels. Since similar phenotypes have been previously described in SOD1 and TDP-43 mutant models, increased axonal growth and branching might represent broad early events in the pathogenesis of ALS.

Keywords

Amyotrophic lateral sclerosis; FUS; HuD; ELAVL4; FMR1; FMRP; NRN1; GAP43; iPSC; motoneuron; axon; 3'UTR.

INTRODUCTION

The motoneuron disease amyotrophic lateral sclerosis (ALS) has been linked to mutations in several RNA binding proteins (RBPs), including the FUS gene, and altered RNA metabolism [1]. Despite a recent increase in our knowledge of the genetics of ALS, the disease mechanisms downstream of mutations in ALS-genes remain largely uncharacterized. In the RBP FUS the most severe ALS mutations, including the P525L, lie within its C-terminal nuclear localization signal (PY-NLS domain), impairing the interaction with the nuclear import receptor Transportin-1 (TNPO1) and reducing nuclear localization [2]. Loss of ALS-linked RBPs nuclear functions, including regulation of alternative splicing and polyadenylation, has been proposed as a pathological ALS mechanism [3-5]. Insoluble cytoplasmatic aggregates containing ALS-linked RBPs are a hallmark of the pathology [6], and gain of toxic cytoplasmic functions may also play important roles in ALS [7].

We previously observed strong correlation between changes in protein levels and selective binding of mutant FUS to 3′UTR [8], suggesting that aberrant targeting of 3′UTRs by mutant FUS likely represents a broad mechanism underlying proteome alteration in motoneurons (MNs). This is particularly relevant for ALS-linked genes, genes encoding for cytoskeletal proteins and, notably, other RBPs [8,9]. Importantly, cellular levels of ALS-linked RBPs are tightly regulated by both auto-regulation mechanisms [10-12] and cross-regulatory mechanisms [9,12-16]. The neural RBP HuD (encoded by the *ELAVL4* gene), a component of cytoplasmic inclusions in FUS, TDP-43 and sporadic ALS patients [9,14], represents an example of such cross-regulation. We have found aberrantly increased HuD levels in *FUS* mutant MNs due to microRNA-mediated effects, and direct binding of mutant FUS to the *HuD* 3'UTR, by a still uncharacterized mechanism [9,17]. HuD is a neural multi-functional RBP and its overexpression induces increased neurite outgrowth in neuronal cell lines and primary neural progenitor cells [18-20], but whether increased levels of HuD have functional consequences in *FUS* mutant MNs remains unexplored.

Axonal degeneration is a key feature in the ALS pathophysiology and occurs prior to the motor phenotype in patients [21-23]. Despite the underlying pathological mechanisms have not been fully elucidated, it has been proposed that axonal alteration, including aberrantly increased branching, can act as a trigger [24]. The levels of cytoskeletal proteins and factors directing neuron projection are changed in *FUS* mutant human pluripotent stem cell (hiPSC)-derived MNs [8], and aberrantly increased branching and axonal outgrowth have been recently identified across ALS mutations and model systems, underlying their importance in early disease pathogenesis [24-28]. Spinal MNs isolated from adult *SOD1* mutant mice at pre-symptomatic stages displayed significant increase in axon outgrowth, in terms of length and branching complexity, and acute expression of mutant SOD1 in WT MNs was sufficient to increase axonal regeneration [29]. These evidences point to axonal alteration as an early, pre-symptomatic phenotype in ALS.

In this work we aimed to gain insight into the molecular mechanisms leading to HuD upregulation in FUS mutant genetic background, and into the functional consequences of HuD increase in MNs. We provide a mechanistic link between increased axon branching and growth upon axotomy and alteration of a cross-regulatory circuitry involving three RBPs: FUS, HuD and the fragile X mental retardation protein (FMRP). We find that FMRP is a negative regulator of *HuD* translation via 3'UTR binding. We propose that this function is outcompeted by mutant FUS binding to the same regulatory region, leading to an increase in HuD protein level, thus providing a mechanistic explanation of HuD upregulation in *FUS* mutant MNs. Further, we identify altered axonal growth as a functional consequence of HuD upregulation, and finally find it to be mediated by the alteration of the HuD target NRN1.

RESULTS

ALS mutant FUS competes with FMRP for *HuD* regulation via 3'UTR binding

We have previously found mutant FUS expression to lead to an increase in HuD [9,17]. Although miR-375 may play a role [17,30], experiments conducted in the absence of miR-375 indicate that a further regulation mechanism is also present. Interestingly, *HuD* 3'UTR is extensively conserved in vertebrates, with a high phyloP100way score (mean: 4.8; standard deviation: 2.3), approaching that of coding exons (e.g. exon 2, mean: 5.9; standard deviation: 3.2) and not restricted to miR-375 binding sites (Supplementary Figure S1), further supporting the existence of another regulatory mechanism.

In order to gain insights into HuD regulation in ALS, we took advantage of spinal MNs derived from isogenic pairs of FUS WT and P525L hiPSC lines (hereafter FUS^{WT} and FUS^{P525L}) by inducible expression of a "programming module" consisting of the transcription factors Ngn2, Isl1 and Lhx3 (NIL) [31,32]. The P525L mutation, localized in the PY-NLS domain (Supplementary Figure S2A), causes severe mislocalization of the FUS protein in the cytoplasm and is often associated to juvenile ALS [2]. In parallel, we used the Fus-Δ14 knock-in mouse model, in which a frameshift mutation leads to the loss of the C-terminal nuclear localization signal (NLS) (Supplementary Figure S2A), causing partial mislocalization to the cytoplasm without altering total Fus protein levels (Supplementary Figure 2B) [33]. In both human *in vitro* MNs (Figure 1A) and mouse spinal cords (post-natal day 81, P81) (Figure 1B), we observed a two-fold increase of HuD protein levels in *FUS* mutant genetic backgrounds. Fluorescence in situ hybridization (FISH) analysis showed a significant increase in the number of *HuD* mRNA puncta in FUS^{P525L} human MNs (Figure 1C). We next took advantage of puro-PLA, a technique that couples puromycylation with the proximity-ligation assay to visualize newly synthesized proteins [34]. Puro-PLA was performed on FUS^{P525L} and FUS^{WT} human MNs using an anti-HuD antibody, revealing an increase in newly synthesized HuD in mutant cells (Figure 1D; Supplementary Figure S3). Increased HuD translation was also detected in primary MNs from the Fus-Δ14 mouse model (Figure 1E).

Together with our previous work [9], these observations suggest that mutant FUS might trigger *HuD* translation upregulation via 3'UTR binding. Mechanistically, this effect could arise from the competition with an inhibitory RBP. We used *cat*RAPID [35] to predict the interactors of the *HuD* 3'UTR. Several RBPs showed interaction propensity with this sequence (Supplementary Table S1), and we filtered this list for ones involved in the regulation of translation (GO:0006412) (Supplementary Table S2). Among these candidates, we focused on negative regulators of translation and noticed FMRP, encoded by the fragile X mental retardation 1 (*FMR1*) gene. Native RNA immunoprecipitation (RIP) was used to validate the physical association between FMRP and the *HuD* transcript. FMRP was effectively immunoprecipitated from hiPSC-derived MN extracts (Figure 2A). A hemizygous FMRP knock-out human iPSC line ($FMRP^{KO}$), generated by CRISPR/Cas9-mediated modification of a male line (hereafter $FMRP^{WT}$) (Supplementary Figure S4) [36], served as a negative control. Quantitative RT-PCR analysis revealed specific enrichment of the *MAP1B* mRNA, a well-characterized FMRP interactor [37,38], and no enrichment of a negative control, the housekeeping *ATP5O* mRNA, in the FMRP immunoprecipitated samples (Figure 2B). Consistent with the *cat*RAPID prediction, FMRP immunoprecipitation enriched the *HuD* mRNA (Figure 2B). Both *MAP1B* and *HuD* were negligible in the immunoprecipitated samples from the control $FMRP^{KO}$ line, confirming the RIP specificity (Supplementary Figure S4D). Notably, *HuD* mRNA levels were reduced in FMRP immunoprecipitated samples from FUS^{P525L} MNs (Figure 2B). Consistent with a previous report [14], we also observed reduced interaction between FMRP and *MAP1B* mRNA in FUS mutant cells (Figure 2B). Decreased interaction with its targets was not consequence of lower FMRP protein level in FUS^{P525L} MNs (Supplementary Figure S4E).

In order to directly assess whether FMRP and mutant FUS compete for *HuD* 3'UTR binding, we set up an *in vitro* binding and competition assay. Three fragments of about 700 nucleotides each, spanning the long *HuD* 3'UTR (F1-F3 in Figure 2C; Supplementary Figure S1), along with a negative control (a portion of the Renilla luciferase coding sequence) were *in vitro* transcribed as

biotinylated RNAs and incubated with HeLa cytoplasmic extract. Upon pull-down with streptavidin beads, western blot analysis revealed strong enrichment of FMRP with F1 and F2, while F3 was not significantly different from the negative control (Figure 2D). We then repeated this experiment for F1 and F2 in presence of the purified recombinant proteins FUS-P525L (RFP-flag-FUS^{P525L}, indicated as P525L in Figure 2E) and FUS-P525L 4F-L, a derivative of the FUS-P525L mutant in which 4 aminoacidic changes impair its RNA binding ability [39] (P525L 4F-L in Figure 2E) (Supplementary Figure S5). For both F1 and F2, we observed strong binding of FUS-P525L, while the RNA-binding defective derivative showed reduced enrichment (Figure 2E). Conversely, FMRP binding was reduced in presence of RNA-binding competent FUS, compared to the 4F-L derivative (statistically significant for F1; Figure 2E).

We then aimed to assess the consequences of impaired FMRP binding to HuD 3'UTR. In MNs obtained from FMRP^{KO} iPSCs, HuD protein levels were increased of approximately two-fold (Figure 3A). In the same cells, HuD transcript levels were unchanged (Figure 3B), suggesting that absence of FMRP upregulated HuD protein without altering its transcription or mRNA stability. In FMRP^{KO} MNs we also observed higher transcript and protein levels of two HuD target genes, *NRN1* and *GAP43* (Figure 3A-B). We next took advantage of a reporter assay to study the outcomes of competitive binding of FMRP and mutant FUS to the *HuD* 3'UTR. We have previously described that expression of a RFP-FUS^{P525L} transgene led to increased translation of a luciferase construct carrying the *HuD* 3'UTR when compared to RFP alone or RFP-FUS^{WT} [9]. We repeated the same experiment upon overexpression of FMRP (or eGFP as a control). As shown in Figure 3C, the *HuD* 3'UTR reporter activity was strongly reduced when FMRP was overexpressed in presence of RFP alone. Notably, co-expression of RFP-FUS^{P525L}, but not RFP-FUS^{WT}, partially reverted such negative regulation by FMRP.

Collectively, these results suggest that FMRP can act as negative regulator of HuD translation in MNs by direct 3'UTR binding. Mutant FUS may intrude in this function by competition for 3'UTR binding, resulting in increased HuD protein levels.

Axon branching and growth phenotypes in FUS mutant MNs

Since HuD protein levels are two- to four-fold higher in human and mouse *FUS* mutant MNs compared to wild-type controls (Figure 1A-B), we wondered if such upregulation could lead to functional consequences. Overexpression of HuD promotes neurite outgrowth in rat PC12 cells (a cell line of neural crest origin) and cortical neurons and, in vivo, in mice overexpressing HuD [18,19,40]. We therefore took advantage of multichambered microfluidics devices to study possible neurodevelopmental defects in *FUS* mutant MNs. FUS^{WT} and FUS^{P525L} human MN progenitors were dissociated and re-plated into one chamber (cell body chamber) of compartmentalized chips with 500 μm microgroove barrier. Such experimental setup allowed us to analyze axons in a separate compartment (axon chamber). Axonal morphology was analyzed after subsequent MN maturation in the device for 7 days. As shown in Figure 4A-B, we found an increased number of axon branches and branch points in the FUS mutant compared to WT (see also Supplementary Figure S6A). A similar increase in axon branching was recently reported by Akiyama and colleagues in MNs derived from human iPSCs carrying a different FUS mutation (H517D) [28]. We further extended this analysis by evaluating axon regeneration after damage. At the sixth day of maturation, chemical axotomy was induced by applying trypsin to the axonal chamber. MNs were then allowed to regenerate their axons for 30 hours. Immunostaining of the neuronal tubulin TUBB3 showed strikingly increased outgrowth in FUS^{P525L} cells (Figure 4C; Supplementary Figure S6B-C). Similar results were obtained when axotomy was induced in the same experimental setup by vacuum application (mechanical injury) or digestion with a different chemical agent, accutase (Figure 4D-E). These results were independently confirmed in the Fus-Δ14 mouse model. Primary embryonic MNs, derived from heterozygous and homozygous mutant mice (E12.5-13.5) and plated in compartmentalized chips, showed increased arborization when compared to WT controls (Figure 5A-B). Increased re-growth was also observed for axotomized *Fus* mutant mouse MNs (Figure 5C).

Increased NRN1 and GAP43 levels in FUS mutant motoneurons

We next focused on downstream HuD targets, which could be altered as a consequence of increased levels of this RBP in FUS mutant MNs, and that might be involved in the observed axon phenotypes. Among the known HuD targets we prioritized *NRN1* and *GAP43*.

HuD stabilizes the mRNA encoding the growth promoting protein NRN1 (Neuritin1) by binding its 3'UTR [41], and we found *NRN1* mRNA levels to be strongly increased in FUS^{P525L} MNs as assessed by quantitative RT-PCR (Figure 6A) and FISH analyses (Figure 6B). Western blot analysis showed that NRN1 protein levels are negligible in FUS^{WT} MNs and increased in FUS^{P525L} cells (Figure 6C). This observation was confirmed in the mouse model, where P81 spinal cord samples showed increased levels of the mouse Nrn1 homolog in heterozygous and homozygous mutants (Figure 6D). Immunostaining analysis in human MNs showed that NRN1 is expressed at low levels in the WT axons and is upregulated in the FUS mutant axons (Figure 6E). Previous work showed that HuD overexpression increased *GAP43* mRNA levels in rat cortical neurons [19]. In particular, HuD binds to an AU-rich regulatory element (ARE) in the 3′UTR of *GAP43* mRNA and stabilizes this transcript [42,43]. As in the case of *NRN1*, increased levels of *GAP43* mRNA were observed in FUS^{P525L} MNs by quantitative RT-PCR and FISH (Figure 6A and Figure 7A). An increase of GAP43 protein levels in the FUS mutant background was detected by western blot analysis in hiPSC-derived MNs but not in mouse spinal cord (Figure 7B-C). The increase in GAP43 protein levels in FUS^{P525L} human MNs was confirmed by immunostaining analysis. Since HuD binding is known to localize GAP43 at growth cones [44], we focused on these structures and found a striking difference: while GAP43 protein was undetectable in FUS^{WT} MNs, a clear punctate signal was present in the FUS^{P525L} mutant (Figure 7D and Supplementary Figure S7A). To a minor extent, difference in GAP43 levels was also found in the MN soma (Supplementary Figure S7B). Increase of *HuD*, *NRN1* and *GAP43* mRNA and protein levels was confirmed in MNs generated from two additional FUS^{P525L} human iPSC lines [45] (Supplementary Figures S8 and S9).

To directly correlate NRN1 and GAP43 upregulation to increased HuD activity, we generated a HuD overexpressing hiPSC line in a FUS^{WT} background. Overexpression of HuD in undifferentiated iPSCs by a constitutive promoter resulted in cell toxicity. We therefore took advantage of a neuronal-specific human synapsin 1 promoter construct (SYN1::HuD) to drive expression of HuD after induction of MN differentiation (Supplementary Figure S10A). The SYN1::HuD construct was stably integrated in FUS^{WT} hiPSCs (FUS^{WT}+HuD in Figure 6A and in Supplementary Figure S10B-E). As a control, we also generated a FUS^{WT} hiPSC line containing SYN1::RFP construct (FUS^{WT}+RFP). These cells were then induced to differentiate to MNs. Rise of HuD in FUS^{WT} SYN1::HuD MNs was in the range of HuD levels observed in FUS^{P525L} MNs. In these cells, we observed increased levels of *NRN1* and *GAP43* mRNA compared to the parental FUS^{WT} line, while no effect was observed in the FUS^{WT}+RFP control (Figure 6A). In the case of *GAP43*, however, change in mRNA levels between FUS^{WT} and FUS^{WT}+HuD did not reach statistical significance. A stronger effect on *NRN1*, compared to *GAP43*, was observed also in $FMRP^{KO}$ MNs, where HuD protein levels were upregulated (Figure 3A-B).

Collectively these data point to increased levels of HuD targets in FUS mutant MNs as a consequence of the disruption of the FMRP-mediated negative regulation of HuD by FUS^{P525L}. In particular, NRN1 is strongly upregulated, while GAP43 is affected in the same direction, although to a minor extent.

Increased axon branching and growth upon axotomy in FUS mutant motoneurons are due to NRN1 upregulation

Given the greater changes in NRN1 levels, compared to GAP43, in FUS mutant MNs, we decided to prioritize this candidate for further analysis. Increased levels of NRN1 in FUS mutant MNs prompted us to explore the possibility that the phenotypes described in Figures 4 and 5 are a direct consequence of aberrant activation of this growth promoting protein. We addressed this hypothesis

by a rescue approach. Small interfering RNAs (siRNAs), transfected during hiPSC-derived MN maturation, effectively reduced NRN1 levels in the FUS^{P525L} background (Figure 8A). In siRNA-NRN1-treated FUS^{P525L} MNs cultured in microfluidics devices we observed reduced number of axon branches and branch points, compared to non-targeting control siRNAs (Figure 8B-C). We next performed in these cells the trypsin-induced axotomy and regeneration assay as in Figure 4C. TUBB3 immunostaining analysis showed that axon growth after regeneration was strongly reduced in FUS^{P525L} MNs treated with NRN1-siRNAs (Figure 8D-E). These results suggest that increased axon branching and growth observed in FUS mutant MNs are mediated by higher levels of NRN1 and that knock-down of NRN1 is sufficient to revert these phenotypes.

DISCUSSION

Here we propose a regulatory mechanism for *HuD* translation in normal MNs and its increase in ALS. A relevant consequence of HuD upregulation in FUS mutant MNs is the increase of two HuD targets: NRN1 and GAP43. In turn, NRN1 hyperactivation confers aberrantly increased axon branching and growth upon axotomy to FUS mutant MNs.

According to our model (Figure 9), a mutation that impairs the nuclear localization of FUS may trigger a domino effect onto other RBPs. One of the consequences is the escape of *HuD* from negative regulation by FMRP on its 3'UTR. The highly conserved *HuD* 3'UTR is indeed a relevant regulatory element, with an important role in keeping HuD protein levels in check. For this purpose, we propose that at least two distinct mechanisms are in place in MNs. The first one involves the activity of the MN-enriched microRNA, miR-375 [17]. The second one, described in this work, relies on the negative regulation of translation by FMRP. Notably, both mechanisms are impaired by FUS mutations. Since *HuD* mRNA levels are affected by miR-375 [9] but not by FMRP (present work), we can conclude that in mutant FUS MNs increased *HuD/ELAVL4* mRNA levels are due to decreased miR-375 expression [17], while increased HuD/ELAVL4 protein levels can be due to the

double effect of the loss of both miR-375 and of FMRP regulation. Interestingly, impaired miR-375 function has been also proposed by others in a mouse model of sporadic ALS [46] and in another MN disease, type1 SMA [47]. In addition to miR-375 and FMRP, our *cat*RAPID analysis indicates that the *HuD* 3'UTR might be also a target of the HuD protein (Supplementary Table S2), thus suggesting possible conservation in human of the autoregulatory mechanism previously proposed in Drosophila and mouse [48,49].

Impairment of FMRP-mediated repression of *HuD* in ALS FUS mutant MNs might occur in several, non-exclusive, possible ways. First, FMRP might be captured in mutant FUS insoluble aggregates, as proposed by Blokhuis and colleagues [14], who also reported impaired FMRP-mediated translational repression and altered MAP1B protein levels in cells overexpressing mutant FUS. In both FUS^{P525L} hiPSC-derived MNs and Fus-Δ14 mice, however, mutant FUS is expressed at physiological levels and does not form aggregates [9,33,50]. Second, FUS mutations might promote phase separation of FMRP by sequestering it in FUS-containing cytoplasmic ribonucleoprotein complexes (RNPs) [51]. Third, mutant FUS might directly compete with FMRP for 3'UTR binding. HuD 3'UTR contains multiple putative regulatory elements and competitive or cooperative 3'UTR binding is a regulatory mechanism extensively used by RBPs [52,53]. Interestingly, loss of the FMRP homolog dFXR leads to NMJ defects in Drosophila [54], while exogenous FMRP expression rescued NMJ and locomotor defects in a zebrafish FUS ALS model [14]. Recent evidence has also linked FMRP with TDP-43 [55,56], suggesting that FMRP involvement in ALS might extend beyond FUS.

Increased HuD suggested a possible underlying mechanism for the increased axon branching and growth phenotypes that we observed in both human and mouse ALS FUS models. HuD has indeed a well-known role in promoting neurogenesis in cell lines and cortical neurons [18,19]. However, to our knowledge, the role of HuD in MNs has never been specifically addressed. Here we show that

at least two relevant HuD targets are upregulated in FUS mutant MNs as a consequence of loss of HuD repression: GAP43 and NRN1. GAP43 is upregulated downstream of increased HuD during axon regeneration upon sciatic nerve injury [44]. In a transgenic mouse model, overexpression of GAP43 induces prolonged nerve sprouting and causes death of adult MNs [57,58]. Together with our present findings, those observations suggest that GAP43 aberrant increase might in part contribute to the pathogenic effects of FUS mutations in ALS MNs.

The growth promoting protein NRN1 is one of the primary HuD targets in MNs. HuD stabilizes NRN1 mRNA via AU-rich element (ARE) binding on its 3'UTR [41,59]. Overall, we observed stronger effects on NRN1 compared to GAP43, at both mRNA and protein levels (with the relevant exception of GAP43 at the growth cone). This is in agreement with previous findings showing that the NRN1 ARE has a higher binding affinity for HuD compared to GAP43 ARE [60]. NRN1, also known as CPG15, was first identified as a candidate plasticity-related gene (CPG) induced by the glutamate analogue kainate in the hippocampus dentate gyrus, along with immediate early genes (IEGs) such as c-Fos and c-Jun [61]. It was later demonstrated that NRN1 is an activity-regulated IEG induced by calcium influx through NMDA receptors and L-type voltage-sensitive calcium channels [62]. Its expression in the rat neocortex peaks at 14 days postnatal and then decreases in the adult [63]. In the adult rat, NRN1 mRNA is detected in brain regions characterized for their activity-modulated plasticity (hippocampus, olfactory bulb and Purkinje cells) and can be induced by glutamate analogs, neurotrophins (such as BDNF) and neural activity [64]. In the Human Protein Atlas [65], the spinal cord is reported among the nervous system regions with lowest NRN1 expression (Supplementary Figure S11). We found increased NRN1 levels in FUS mutant hiPSC-derived MNs and mouse spinal cord, in the absence of promoting stimuli. NRN1 was also upregulated upon HuD overexpression and FMRP knock-out. When overexpressed in rodent or Xenopus neurons, NRN1 induced neurite outgrowth, elaboration of dendritic and axonal arbors and synaptic maturation by AMPA receptor insertion [64,66,67]. Moreover, axonal localization of *Nrn1*

mRNA, which is induced after nerve injury and is mediated by the 3'UTR in central nervous system and by the 5'UTR in peripheral nervous system axons, promotes axon growth [68]. NRN1 is highly expressed in developing MNs, where its overexpression increases axonal outgrowth and neurite branching [69]. This phenotype is remarkably similar to increased neurite outgrowth and branching observed in motor neurons expressing the ALS SOD1-G93A mutant [29]. Consistently, increased axon branching and growth upon axotomy occurring in our mutant FUS models could be rescued by reduction of NRN1 levels with siRNAs. This result suggests that increased NRN1 mRNA stability, downstream of HuD upregulation, may be one of the key aberrant mechanisms underlying the observed axon phenotypes.

Consistent with our findings, Akiyama and colleagues have recently reported an increased axon branching phenotype in iPSC-derived MNs carrying the FUS^{H517D} mutation [28]. They also showed increased levels of AP-1 components (including members of the FOS family) and reversion of the axon branching phenotype upon FOS-B reduction [28]. AP-1 increase might not directly contribute to NRN1 upregulation in FUS mutant cells. In stimulated cortical neurons, indeed, NRN1 upregulation occurred independently from new protein synthesis, indicating that NRN1 induction does not require prior activation of AP-1 [62]. Therefore, the effects observed by Akiyama and colleagues upon modulation of FOS-B are unlikely mediated by NRN1. To the best of our knowledge, NRN1 has been never associated with ALS before. However, by mining published RNA-Seq datasets we found an upregulation trend of the *Nrn1*/*NRN1* transcript in the soma of MNs dissected from a SOD1 mouse model at a pre-symptomatic stage (3 months) [70] or generated from SOD1 mutant human and mouse stem cells [71]. Pro-regenerative effects on adult MNs upon ALS-mutant SOD1 expression have been recently shown, including increased outgrowth and branching [29]. This is unlikely a compensatory response to mutant SOD1-induced toxicity, as it occurs also upon acute expression of mutant SOD1 in WT adult MNs. Notably, MN axon branching was also increased in zebrafish embryos injected with ALS-mutant TDP-43 proteins, which showed a motor

deficit [26]. The importance of aberrant axon branching and growth in ALS pathophysiology deserves more investigation, as it might be detrimental for the normal function of signal transmission in MNs [24]. Notably, recent evidence of HuD upregulation and increased binding activity in sporadic ALS patients' motor cortex [72] suggests that the present findings might extend beyond FUS-ALS. Our work provides insights into the molecular mechanisms underlying such axonal phenotypes in FUS-ALS.

MATERIALS AND METHODS

Plasmids construction

The epB-Puro-TT-SYN1-HuD (SYN1::HuD) and epB-Puro-TT-SYN1-RFP (SYN1::RFP) plasmids were generated by inserting the sequences of the human synapsin 1 (SYN1) promoter and, respectively, Flag-HA-HuD and tagRFP in the enhanced piggyBac transposable vector epB-Puro-TT [73]. The SYN1 promoter was isolated from the eMSCL WT plasmid (Addgene, #107454) via PCR with the following primers: hSYN1 FW 5'-CATCTCGAGCAGTGCAAGTGGGTTTTAGGAC-3'; hSYN1 RV 5'-CATGGATCCACTGCGCTCTCAGGCACGA-3'. Flag-HA-HuD was obtained by cutting the pFRT-TODestFLAGHA_HuD plasmid (Addgene, #65757) with PaeI and BglII enzymes. Such HuD sequence is devoid of both 5' and 3'UTR. The resulting constructs contain the enhanced piggyBac terminal repeats flanking a constitutive cassette driving the expression of the puromycin resistance gene fused to the rtTA gene and, in the opposite direction, a SYN1 promoter driving the expression of the transgenes (Supplementary Figure S10). The ePB-Bsd-TT-FMR1 and ePB-Bsd-TT-eGFP plasmids were generated by subcloning the FMR1 and eGFP coding sequences, respectively, in the enhanced piggyBac transposable vector epB-Bsd-TT [9]. The epB-NIL vector for spinal MN differentiation, containing the Ngn2, Isl1 and Lhx3 transgenes, is described in [31].

iPSC culture, differentiation and transfection

Generation of the hiPSC lines WT I and FUS-P525L/P525L is described in [50]. KOLF iPSCs WT 2 and P525L16 (LL FUS-eGFP) and T12.9 iPSCs WT15 and P525L17 (SL FUS-eGFP) are a kind gift of J. Sterneckert [45]. The FMR1 KO hiPSC line was generated by CRISPR/Cas9 gene editing from the WT I line, as described in [36] and in Supplementary Figure S4. Maintenance conditions of iPSCs are described in [50]. iPSCs were co-transfected with 4.5 µg of transposable vector (epB-NIL, SYN1::HuD, SYN1::RFP) and 0.5 µg of the piggyBac transposase using the Neon Transfection System (Life Technologies), as described [50]. Selection was carried out in 5 µg/ml blasticidin S (for epB-NIL) and 1 µg/ml puromycin (for SYN1::HuD, SYN1::RFP), giving rise to stable cell lines.

The spinal MN differentiation protocol is detailed in [31,32]. Briefly, epB-NIL-containing cells were differentiated upon induction with 1 µg/ml doxycycline (Thermo Fisher Scientific) in DMEM/F12 (Sigma-Aldrich), supplemented with 1X Glutamax (Thermo Fisher Scientific), 1X NEAA (Thermo Fisher Scientific) and 0.5X Penicillin/Streptomycin (Sigma-Aldrich) for 2 days and Neurobasal/B27 medium (Neurobasal Medium, Thermo Fisher Scientific; supplemented with 1X B27, Thermo Fisher Scientific; 1X Glutamax, Thermo Fisher Scientific; 1X NEAA, Thermo Fisher Scientific; and 0.5X Penicillin/Streptomycin, Sigma Aldrich), containing 5 µM DAPT and 4 µM SU5402 (both from Sigma-Aldrich) for additional 3 days. At day 5, MN progenitors were dissociated with Accutase (Thermo Fisher Scientific) and plated on Matrigel (BD Biosciences)-coated 15 mm diameter dishes or cover glass (0.13-0.17 thick), or bipartite/tripartite microfluidic chambers (MFCs, see below) at the density of 10^5 cells per cm^2. 10 µM rock inhibitor was added for the first 24 hours after dissociation. Neuronal cultures were maintained in neuronal medium (Neurobasal/ B27 medium supplemented with 20 ng/ml BDNF and 10 ng/ml GDNF, both from PreproTech; and 20 ng/ml L-ascorbic acid, Sigma-Aldrich). MFCs were made with Sylgard 184 silicone elastomer kit (Dow Corning) using epoxy resin molds. Once the MFCs were baked, reservoirs were cut and the MFCs were mounted onto glass-bottom dishes (HBST-5040, WillCo well), pre-coated with 1:200 100X poly-D-Lysine. MFCs were then blocked with 0.8% BSA in ES

(Sigma-Aldrich) overnight and then coated with Matrigel (BD Biosciences), before plating MN progenitors. MFCs have 500 μm long grooves that separate the somatic from the axonal compartment.

Mouse primary motoneurons

Fus-Δ14 mice (B6N;B6J-Fus$^{tm1Emcf/H}$, MGI: 6100933) were previously described [33]. All applicable international, national, and institutional guidelines, including ARRIVE guidelines, for the care and use of animals were followed. All procedures performed in studies involving animals were in accordance with the ethical standards of the institution at which the studies were conducted (University College London, UK; MRC Harwell Institute, Oxfordshire, UK). All procedures for the care and treatment of animals were in accordance with the Animals (Scientific Procedures) Act 1986 Amendment Regulations 2012. Primary MNs (PMNs) were isolated from E12.5-13.5 mouse embryos on a congenic C57BL/6J background. Briefly, embryos were euthanized, spinal cord removed and ventral regions isolated. PMNs were dissociated by incubation with trypsin, followed by mechanical dissociation in combination with DNase treatment. Cells were then centrifuged through a bovine serum albumin (BSA) cushion and resuspended in motor neuron medium (Neurobasal; Thermo Fisher, Waltham, MA), 2% v/v B27 supplement (Thermo Fisher Scientific), 2% heat-inactivated horse serum (HRS), 1X GlutaMAX (Thermo Fisher Scientific), 24.8 μM β-mercaptoethanol, 10 ng/ml rat ciliary neurotrophic factor (CNTF; R&D Systems), 0.1 ng/ml rat glial cell line-derived neurotrophic factor (GDNF; R&D systems), 1 ng/ml human brain-derived neurotrophic factor (BDNF; PeproTech) and 1% penicillin/streptomycin. PMNs were immediately plated on poly-L-ornithine/laminin- coated plates or MFCs and cultured for 6-7 days at 37°C in a 5% CO_2 incubator.

Adult spinal cord samples were collected from female Fus-Δ14 mice on a (C57BL/6J x DBA/2J) F1 hybrid background, via laminectomy, and snap frozen over liquid nitrogen. The hybrid background

was necessary to produce viable homozygotes, which are non-viable on a congenic C57BL/6J background.

Western blot

Western blot analysis was carried out using anti-HuD (1:1000; sc-48421, Santa Cruz), anti-NEURITIN (1:200; AF283, R&D Systems), anti-GAP43 (1:500; LS-C356053, Bio-techne) (for human samples), anti-GAP-43 (1:500; 5307, Cell Signaling Technology) (for mouse samples), anti-flag (1:1000; F3165, Sigma-Aldrich), anti-TUBB3 (1:10000; T2200, Sigma-Aldrich), anti-GAPDH (1:2000; MAB-10578 Immunological sciences) primary antibodies and donkey anti-mouse IgG (H+L) (IS20404; Immunological Science) and donkey anti-rabbit IgG (H+L) (IS20405; Immunological Science) secondary antibodies, as previously described [9].

Real-time qRT-PCR

Total RNA, extracted with the RNA extract kit ($1x10^6$ cells-10mg; VWR International PBI) and retrotranscribed with iScript Supermix (Bio-Rad Laboratories), was analyzed by real-time qRT-PCR with iTaq Universal SYBR Green Supermix (Bio-Rad Laboratories). *ATP5O* was used as the internal calibrator. Primers sequences are listed in Supplementary Table S3.

RNA interference (RNAi)

NRN1 RNAi was induced with a synthetic siRNA pool targeting the human NRN1 mRNA (NRN1 51299 siRNA-SMARTpool, Dharmacon) or with a non-targeting siRNA control pool with scrambled sequence (ON-TARGETplus Non-targeting Pool; D-001810-10-05, Dharmacon). Lyophilized siRNAs were resuspended in nuclease-free water and stored at –20 °C as 20 μM stocks until use. For transfection, siRNAs were diluted in Optimem (Gibco) and mixed with siLentFect Lipid Reagent (Bio-Rad Laboratories), according to the protocol for transfection of adherent cells.

The final siRNA concentration in each MFC was 10 nM. Medium was changed 5 hours post-transfection.

Immunofluorescence

Cells were fixed in 4% paraformaldehyde (PFA) in PBS for 10 min at room temperature. Coverslips were washed with PBS, permeabilized and blocked for 15 min using a solution of 0.5% BSA, 10% HRS, 0.2% Triton X-100 in PBS (all from Sigma-Aldrich). Anti-TUJ1 (for TUBB3 detection; 1:1000; T2200, Sigma-Aldrich), anti-GAP-43 (1:500; LS-C356053, Bio-techne), anti-MAP2 (1:2000; ab5392, Abcam), anti-NEURITIN (1:200; AF283, R&D Systems), anti-488-PHALLOIDIN (1:50; 49429, Sigma-Aldrich), Anti-TYR-TUBULIN clone YL1/2 (1:1000; MAB1864-I, Sigma-Aldrich) antibodies were diluted in a solution of 0.5% BSA, 10% HRS in PBS and incubated with the cells for 1 hour at room temperature. Cells were then washed in PBS and incubated for 1 hour at room temperature with the appropriate fluorescent conjugated secondary antibodies: anti-mouse Alexa Fluor 488 (1:200, Thermo Fisher Scientific), anti-rabbit Alexa Fluor 594 (1:200, Immunological Sciences) and anti-goat Alexa Fluor 594 (1:200, Immunological Sciences) produced in donkey; anti-Rat IgG (H+L), highly cross-adsorbed, CF™ 647 secondary antibody (1:500; SAB4600186, Sigma-Aldrich) produced in goat; DAPI (1:2000; Sigma-Aldrich) diluted in 0.5% BSA, 10% HRS in PBS. Finally, cells were washed with PBS, mounted using DAKO mounting media and imaged using inverted Zeiss LSM 780 or 510 confocal microscopes using a 63×, 1.4 NA DIC Plan-Apochromat oil-immersion objective, except for images shown in Figure 8D, which have been acquired with an inverted Olympus iX73 equipped with an X-Light V3 spinning disc head (Crest Optics), a LDI laser illuminator using 470 nm wavelength (89 North), a CoolSNAP MYO CCD camera (Photometrics) and MetaMorph software (Molecular Devices) with a 10× objective.

Puro-PLA

Cells were treated with either DMSO or 40 μM anisomycin for 30 min. Then, 2 μM puromycin was added to the medium for 7 min at 37°C in a 5% CO_2 incubator, cells were washed 2 times with PBS and fixed in 4% PFA in PBS for 12 min at room temperature. Coverslips were permeabilized with 0.2% Triton X-100 in PBS for 15 min and blocked using a solution of 0.5% BSA and 10% HRS in PBS for 30 min. Detection of newly synthesized proteins was carried out by an anti-puromycin antibody (clone 12D10, mouse-monoclonal, MABE343; Merck), an anti-HuD antibody (ab96474, rabbit-monoclonal; Abcam) and Duolink PLA Fluorescence reagents Red (DUO92008, Duolink), according to manufacturer's instructions, using rabbit PLAplus (DUO92002, Duolink) and mouse PLAminus (DUO92004, Duolink). The anti-TUJ1 antibody was used as a cell marker and to identify axons, as described in the 'Immunofluorescence' section. All samples were mounted in Duolink In Situ Mounting Media with DAPI (DUO82040, Duolink).

Fluorescence in situ hybridization (FISH)

Cells were fixed for 15 min with 4% PFA in PBS. FISH was performed with the QuantiGene ViewRNA ISH Cell Assay (Thermo Fisher Scientific) protocol for adherent cells. Briefly, fixed MNs were rinsed 3 times in PBS containing 5 mM $MgCl_2$ for 5 min. Cells were then dehydrated in ethanol (50%,75%,100%) for 2 min each and stored at -20°C for up to one week, minimum of 2 hours. Coverslips were rehydrated (75%, 50%) for 2 min each and washed 3 times in PBS containing 5 mM $MgCl_2$ for 5 min. Coverslips were permeabilized with Detergent Solution and then treated with Protease QS (1:8000). FISH was carried out following manufacturer's instructions (QVC000; Thermo Fisher Scientific). Cells were mounted using DAKO mounting media or Prolong Gold with DAPI (Invitrogen) and imaged using an inverted Zeiss LSM 780 or 510 confocal microscope using a 63X, 1.4 NA DIC Plan-Apochromat oil-immersion objective and Zeiss LSM 880 laser scanning confocal microscope.

RNA immunoprecipitation (RIP)

iPSC-derived motor neurons at day 12 of differentiation were lysed with PLB Buffer (5 mM $MgCl_2$, 10 mM HEPES (pH 7.0), 150 mM KCl, 5 mM EDTA (pH 8), 0.5% NP-40, 2 mM DTT, with 100 U/ml RNAase inhibitor and 1X protease inhibitor cocktail), incubated for 5 minutes on ice and centrifuged 10 minutes at 4°C at 14000g. Protein concentration of the supernatant was then measured by Bradford assay and a volume containing 1 mg of proteins was diluted in NT2 Buffer (50 mM Tris (pH 7), 150 mM NaCl, 0.5 mM $MgCl_2$, 0.05% NP-40, 1 mM DTT, 20 mM EDTA (pH 8) with 100 U/ml RNAse inhibitor and 1X protease inhibitor cocktail). Protein G-coupled dynabeads (immunoprecipitation kit, Invitrogen) were washed in NT2 Buffer, incubated with 10 µg of anti-FMRP (f4055, Sigma Aldrich), anti-FMRP (ab17722, Abcam) or rabbit monoclonal anti-human IgG antibody (ab109489, Abcam) and left rotating on a wheel for 1 hour at room temperature in NT2 Buffer. Beads were then washed in NT2 Buffer and incubated with the diluted lysates in a final volume of 500 µl. Binding was carried out at 4°C with the samples rotating on a wheel for 2 hours. Beads were then washed 3 times and resuspended in ice-cold NT2. Each sample was split 1/5 for protein and 4/5 for RNA analysis. The protein fraction was resuspended in 1X NuPage LDS (Invitrogen) with 2 mM DTT and left at 70°C for 20 minutes. Proteins were run on a 4%–12% polyacrylamide gel for 1 hour at 160 V. An artificial spike RNA, i.e. an *in vitro* transcribed RNA fragment derived from the pcDNA3.1 plasmid, was added to the RNA fraction, which was then lysed with 250 µl of TRIzol (Invitrogen) and extracted according to manufacturer's instructions. RNA was analyzed by real-time qRT-PCR with iTaq Universal SYBR Green Supermix (Bio-Rad Laboratories). RIP data analysis was performed as follows. For each target, the mean Ct value from a technical duplicate was normalized to the input RNA fraction (at a 1/10 dilution) Ct value (ΔCt) to account for RNA sample preparation differences, using the equation: $\Delta Ct = [Ct_{RIP\ or\ IgG} - Ct_{input} - Log_2 10]$. The percentage of input was calculated by linear conversion of the normalized ΔCt as $2^{-\Delta Ct}$. This value was then adjusted to take into account the difference in the amplification between the control IgG and the IP fractions using the artificial spike RNA, as follows. We first calculated the spike RNA ΔCt and percentage of input as described above. Then,

we normalized the percentage of input of each target using the percentage of input of the spike RNA.

In vitro binding and competition assays

In vitro binding assay was performed using *in vitro* transcribed biotinylated RNA (corresponding to 3 regions spanning the *HuD* 3'UTR), HeLa extract (containing FMRP protein), and purified recombinant FUS proteins form HeLa, as follows.

For *HuD* 3'UTR fragments, biotinylated RNA preparation was carried out using PCR products generated from hiPSC-FUS^{WT} gDNA. The forward PCR primers contained the T7 RNA polymerase promoter sequence (T7): TAATACGACTCACTATAGGG. Primers sequences are listed in Supplementary Table S3. For the RNA negative control, a DNA fragment containing the T7 promoter was obtained by cutting the pSI-Check2 vector with EcoRV and HindIII. These DNA templates were used for *in vitro* RNA transcription with the T7 polymerase MAXIscript kit (Invitrogen), in presence of 0.2 mM Biotin-16-UTP (Roche). RNA was purified by adding one volume per sample of phenol:chloroform:isoamyl alcohol (25:24:1) (Thermo Fisher), followed by centrifugation at 4°C for 10 minutes at 1000 rpm and precipitation of the upper aqueous phase with ethanol at -80°C overnight.

For biotin pull-down, Streptavidin MagneSphere paramagnetic particles (Promega) were first washed in EMSA buffer 1X (EMSA buffer 2X: 40 mM Hepes pH 7.9, 150 mM KCl, 3mM $MgCl_2$, 2 mM DTT, 10% glycerol with 100 U/ml RNAse inhibitor and 1X protease inhibitor cocktail; Roche) four times. Beads were then incubated in EMSA 1X with 150 µg of E. Coli tRNA at RT for 10 minutes. After the treatment, the beads were resuspended in EMSA 1X with 100 U/ml RNAse inhibitor and 1X protease inhibitor cocktail (Roche). FRMP binding assay was performed by incubating biotinylated transcripts (250 ng) and 75 µg of HeLa cytoplasmic lysate for 30 minutes on ice in EMSA buffer 1X.

FUS protein purification for competition assays was performed as follows. Stable and inducible RFP-flag-FUS^{P525L} and RFP-flag-4FL_FUS^{P525L} HeLa lines were induced with 200 ng/µl doxycycline for 24 hours. Cells were lysed with RIPA buffer (50 mM Tris–HCl pH 7.5, 150 mM NaCl, 1% NP-40, 0.5% sodium deoxycholate, 0.1% SDS, 1 mM EDTA, 1 mM EGTA and 1X protease inhibitor cocktail; Roche). Anti-FLAG M2 Magnetic Beads (Sigma Aldrich) were washed in Tris Buffer Saline (TBS) two times. A volume containing 5 mg of protein extract was incubated with beads and binding was carried out at 4°C on a rotating wheel overnight. Beads were then washed in Low buffer (50 mM Tris HCl pH 7.5, 150 mM NaCl, 1 mM EDTA, 5% glycerol, 0,25% NP40) three times and in High buffer (50 mM Tris HCl pH 7.5, 500 mM NaCl, 1 mM EDTA, 5% glycerol, 0,25% NP40) two times. Beads were then resuspended in TBS with Flag peptide (Millipore) in final volume of 50 µl and left at 4°C on a rotating wheel for 5 minutes. This step was repeated three times, obtaining three different elution samples. Each sample (1/10) was resuspended in 1X NuPage LDS (Invitrogen) with 2 mM DTT and left at 70°C for 10 minutes. Proteins were run on a 4%–12% polyacrylamide gel for 1 hour at 150 V and colored with PageBlue Protein staining solution (Thermo Scientific) overnight.

For competition assay between FMRP and FUS, Streptavidin MagneSphere paramagnetic particles (Promega) were first washed in EMSA buffer 1X four times. Beads were then incubated in EMSA 1X with 150 µg of E. Coli tRNA at RT for 10 minutes and resuspended in EMSA 1X with 100 U/ml RNAse inhibitor and 1X protease inhibitor cocktail (Roche). The assay was then performed in presence of 250 ng of biotinylated transcript, 75 µg of HeLa cytoplasmic lysate and 30 ng of purified FUS protein. RNA-protein complexes were then incubated with streptavidin beads in a final volume of 150 µl. Binding was carried out at 4°C with on a rotating wheel for 1 hour. Beads were then washed in 1X EMSA for three times. Each sample was resuspended in 20 µl PBS with 1X NuPage LDS (Invitrogen) and 2 mM DTT. Complexes were analyzed by western blotting.

Luciferase assay

The pSI-Check2 vector containing HuD 3'UTR (RLuc-HuD 3'UTR) is described in [9]. RLuc-HuD 3'UTR was transfected alone or in combination with epB-Bsd-TT-FMR1 or epB-Bsd-TT-eGFP in $5x10^4$ pre-seeded HeLa cells expressing RFP-FUS^{P525L} [9] in a 24-well plate using Lipofectamine 2000 (Life Technologies), following manufacturer's instructions. Cells were harvested 24 hours post-transfection and RLuc and FLuc activities were measured by Dual Glo luciferase assay (Promega), according to the manufacturer's protocol.

Axon branching and growth upon axotomy assays

After dissociation at day 5 of differentiation, hiPSC-derived MNs were grown in microfluidics for 7 days. For axon branching analysis, the initial density was $5x10^4$ cells per cm^2. For axotomy experiments, the initial density was 10^5 cells per cm^2. Axotomy was performed using 3 different methods: 1) Trypsin-EDTA 0.25% (Thermo Fisher Scientific) treatment for 15 min (Figure 4C, 5C, 8C; Supplementary Figure 5A); 2) repeated vacuum aspirations (Figure 4D); 3) Accutase (Thermo Fisher Scientific) treatment for 15 min (Figure 4E). The axon chamber was reperfused with PBS until effective removal of the damaged axons, without disturbing the cell bodies in the soma compartment.

Quantitative analyses of axon branches and branch points were conducted with Skeleton, a plugin of Fiji [74]. 30 hours after axotomy, immunofluorescence staining with an anti-TUJ1 antibody was performed as described in the 'Immunofluorescence' section.

Statistics and Reproducibility

Statistical analysis, graphs and plots were generated using GraphPad Prism 6 (GraphPad Software). As indicated in each figure legend, Student's t-test or ordinary one-way ANOVA was performed, and data set are shown in dot plots indicating mean ± standard deviation (st.dev.) or standard error of the mean (s.e.m.). Sample size for each experiment is also indicated in the figure legends.

Data availability

All data generated or analyzed during this study are included in this published article and its supplementary information files.

COMPETING INTERESTS

The authors declare that they have no competing interests.

FUNDING

This work was partially supported by Sapienza University, Fondazione Istituto Italiano di Tecnologia and a grant from Istituto Pasteur Italia - Fondazione Cenci Bolognetti to A.R. P.F., T.J.C., R.R.N. and E.M.C.F., were funded by grants from the UK Medical Research Council.

AUTHORS' CONTRIBUTIONS

Conceptualization, M.G.G., M.R. and A.R.; Formal analysis, M.G.G., N.B., M.R.; Investigation, M.G.G., N.B., F.S.; Methodology, M.G.G., F.S., Mi.Mo., V.d.T., R.R.N., M.R, Ma.Mo.; Project administration, A.R.; Supervision, A.R., P.F., E.M.C.F. and T.J.C.; Writing – original draft, A.R.

All authors read and approved the final manuscript.

ACKNOWLEDGMENTS

The authors wish to thank the Imaging Facility at Center for Life Nano Science, Istituto Italiano di Tecnologia, for support and technical advice. We are grateful to Jared Sterneckert (Technische Universität Dresden, Germany) for sharing their human iPSC lines. We thank Riccardo De Santis (The Rockefeller University, NY, USA), Serena Carra (University of Modena and Reggio Emilia, Italy) and Silvia Di Angelantonio and Irene Bozzoni (Sapienza University of Rome, Italy) for helpful discussion.

REFERENCES

1. Brown RH, Al-Chalabi A. Amyotrophic Lateral Sclerosis. *N Engl J Med* 2017; **377**: 162–172.

2. Dormann D, Rodde R, Edbauer D, Bentmann E, Fischer I, Hruscha A *et al.* ALS-associated fused in sarcoma (FUS) mutations disrupt Transportin-mediated nuclear import. *EMBO J* 2010; **29**: 2841–2857.

3. Lagier-Tourenne C, Polymenidou M, Hutt KR, Vu AQ, Baughn M, Huelga SC *et al.* Divergent roles of ALS-linked proteins FUS/TLS and TDP-43 intersect in processing long pre-mRNAs. *Nat Neurosci* 2012. doi:10.1038/nn.3230.

4. Klim JR, Williams LA, Limone F, Guerra San Juan I, Davis-Dusenbery BN, Mordes DA *et al.* ALS-implicated protein TDP-43 sustains levels of STMN2, a mediator of motor neuron growth and repair. *Nature Publishing Group* 2019; **22**: 167–179.

5. Melamed Z, López-Erauskin J, Baughn MW, Zhang O, Drenner K, Sun Y *et al.* Premature polyadenylation-mediated loss of stathmin-2 is a hallmark of TDP-43-dependent neurodegeneration. *Nature Publishing Group* 2019; **22**: 180–190.

6. Dormann D, Haass C. TDP-43 and FUS: a nuclear affair. *Trends in neurosciences* 2011; **34**: 339–348.

7. Birsa N, Bentham MP, Fratta P. Cytoplasmic functions of TDP-43 and FUS and their role in ALS. *Semin Cell Dev Biol* 2019. doi:10.1016/j.semcdb.2019.05.023.

8. Garone MG, Alfano V, Salvatori B, Braccia C, Peruzzi G, Colantoni A *et al.* Proteomics analysis of FUS mutant human motoneurons reveals altered regulation of cytoskeleton and other ALS-linked proteins via 3'UTR binding. *Sci Rep* 2020; **10**: 11827.

9. De Santis R, Alfano V, de Turris V, Colantoni A, Santini L, Garone MG *et al.* Mutant FUS and ELAVL4 (HuD) Aberrant Crosstalk in Amyotrophic Lateral Sclerosis. *Cell Rep* 2019; **27**: 3818–3831.e5.

10. Ayala YM, De Conti L, Avendaño-Vázquez SE, Dhir A, Romano M, D'Ambrogio A *et al.* TDP-43 regulates its mRNA levels through a negative feedback loop. *EMBO J* 2011; **30**: 277–288.

11. Zhou Y, Liu S, Liu G, Oztürk A, Hicks GG. ALS-associated FUS mutations result in compromised FUS alternative splicing and autoregulation. *PLoS Genet* 2013; **9**: e1003895.

12. Humphrey J, Birsa N, Milioto C, McLaughlin M, Ule AM, Robaldo D *et al.* FUS ALS-causative mutations impair FUS autoregulation and splicing factor networks through intron retention. *Nucleic Acids Res* 2020. doi:10.1093/nar/gkaa410.

13. Huelga SC, Vu AQ, Arnold JD, Liang TY, Liu PP, Yan BY *et al.* Integrative genome-wide analysis reveals cooperative regulation of alternative splicing by hnRNP proteins. *Cell Rep* 2012; **1**: 167–178.

14. Blokhuis AM, Koppers M, Groen EJN, van den Heuvel DMA, Dini Modigliani S, Anink JJ *et al.* Comparative interactomics analysis of different ALS-associated proteins identifies converging molecular pathways. *Acta Neuropathol* 2016; **132**: 175–196.

15. Mohagheghi F, Prudencio M, Stuani C, Cook C, Jansen-West K, Dickson DW *et al.* TDP-43 functions within a network of hnRNP proteins to inhibit the production of a truncated human SORT1 receptor. *Hum Mol Genet* 2016; **25**: 534–545.

16. Gueroussov S, Weatheritt RJ, O'Hanlon D, Lin Z-Y, Narula A, Gingras A-C *et al.* Regulatory Expansion in Mammals of Multivalent hnRNP Assemblies that Globally Control Alternative Splicing. *Cell* 2017; **170**: 324–339.e23.

17. De Santis R, Santini L, Colantoni A, Peruzzi G, de Turris V, Alfano V *et al.* FUS Mutant Human Motoneurons Display Altered Transcriptome and microRNA Pathways with Implications for ALS Pathogenesis. *Stem Cell Reports* 2017; **9**: 1450–1462.

18. Anderson KD, Morin MA, Beckel-Mitchener A, Mobarak CD, Neve RL, Furneaux HM *et al.* Overexpression of HuD, but not of its truncated form HuD I+II, promotes GAP-43 gene expression and neurite outgrowth in PC12 cells in the absence of nerve growth factor. *Journal of neurochemistry* 2000; **75**: 1103–1114.

19. Anderson KD, Sengupta J, Morin M, Neve RL, Valenzuela CF, Perrone-Bizzozero NI. Overexpression of HuD accelerates neurite outgrowth and increases GAP-43 mRNA expression in cortical neurons and retinoic acid-induced embryonic stem cells in vitro. *Exp Neurol* 2001; **168**: 250–258.

20. Tebaldi T, Zuccotti P, Peroni D, Köhn M, Gasperini L, Potrich V *et al.* HuD Is a Neural Translation Enhancer Acting on mTORC1-Responsive Genes and Counteracted by the Y3 Small Non-coding RNA. *Mol Cell* 2018; **71**: 256–270.e10.

21. Fischer LR, Culver DG, Tennant P, Davis AA, Wang M, Castellano-Sanchez A *et al.* Amyotrophic lateral sclerosis is a distal axonopathy: evidence in mice and man. *Exp Neurol* 2004; **185**: 232–240.

22. Roy S, Zhang B, Lee VM-Y, Trojanowski JQ. Axonal transport defects: a common theme in neurodegenerative diseases. *Acta Neuropathol* 2005; **109**: 5–13.

23. Ferraiuolo L, Kirby J, Grierson AJ, Sendtner M, Shaw PJ. Molecular pathways of motor neuron injury in amyotrophic lateral sclerosis. *Nat Rev Neurol* 2011; **7**: 616–630.

24. Suzuki N, Akiyama T, Warita H, Aoki M. Omics Approach to Axonal Dysfunction of Motor Neurons in Amyotrophic Lateral Sclerosis (ALS). *Front Neurosci* 2020; **14**: 194.

25. McWhorter ML, Monani UR, Burghes AHM, Beattie CE. Knockdown of the survival motor neuron (Smn) protein in zebrafish causes defects in motor axon outgrowth and pathfinding. *J Cell Biol* 2003; **162**: 919–931.

26. Kabashi E, Lin L, Tradewell ML, Dion PA, Bercier V, Bourgouin P *et al.* Gain and loss of function of ALS-related mutations of TARDBP (TDP-43) cause motor deficits in vivo. *Hum Mol Genet* 2010; **19**: 671–683.

27. Hogan AL, Don EK, Rayner SL, Lee A, Laird AS, Watchon M *et al.* Expression of ALS/FTD-linked mutant CCNF in zebrafish leads to increased cell death in the spinal cord and an aberrant motor phenotype. *Hum Mol Genet* 2017; **26**: 2616–2626.

28. Akiyama T, Suzuki N, Ishikawa M, Fujimori K, Sone T, Kawada J *et al.* Aberrant axon branching via Fos-B dysregulation in FUS-ALS motor neurons. *EBioMedicine* 2019; **45**: 362–378.

29. Osking Z, Ayers JI, Hildebrandt R, Skruber K, Brown H, Ryu D *et al.* ALS-Linked SOD1 Mutants Enhance Neurite Outgrowth and Branching in Adult Motor Neurons. *iScience* 2019; **11**: 294–304.

30. Abdelmohsen K, Hutchison ER, Lee EK, Kuwano Y, Kim MM, Masuda K *et al.* miR-375 inhibits differentiation of neurites by lowering HuD levels. *Mol Cell Biol* 2010; **30**: 4197–4210.

31. De Santis R, Garone MG, Pagani F, de Turris V, Di Angelantonio S, Rosa A. Direct conversion of human pluripotent stem cells into cranial motor neurons using a piggyBac vector. *Stem Cell Research* 2018; **29**: 189–196.

32. Garone MG, de Turris V, Soloperto A, Brighi C, De Santis R, Pagani F *et al.* Conversion of Human Induced Pluripotent Stem Cells (iPSCs) into Functional Spinal and Cranial Motor Neurons Using PiggyBac Vectors. *J Vis Exp* 2019. doi:10.3791/59321.

33. Devoy A, Kalmar B, Stewart M, Park H, Burke B, Noy SJ *et al.* Humanized mutant FUS drives progressive motor neuron degeneration without aggregation in 'FUSDelta14' knockin mice. *Brain* 2017; **140**: 2797–2805.

34. tom Dieck S, Kochen L, Hanus C, Heumüller M, Bartnik I, Nassim-Assir B *et al.* Direct visualization of newly synthesized target proteins in situ. *Nat Methods* 2015; **12**: 411–414.

35. Agostini F, Zanzoni A, Klus P, Marchese D, Cirillo D, Tartaglia GG. catRAPID omics: a web server for large-scale prediction of protein-RNA interactions. *Bioinformatics* 2013; **29**: 2928–2930.

36 Brighi C, Salaris F, Soloperto A, Cordella F, Ghirga S, de Turris V *et al*. Novel fragile X syndrome 2D and 3D brain models based on human isogenic FMRP-KO iPSCs. *Cell Death and Disease* 2021; **12**:498.

37. Brown V, Jin P, Ceman S, Darnell JC, O'Donnell WT, Tenenbaum SA *et al.* Microarray identification of FMRP-associated brain mRNAs and altered mRNA translational profiles in fragile X syndrome. *Cell* 2001; **107**: 477–487.

38. Darnell JC, Jensen KB, Jin P, Brown V, Warren ST, Darnell RB. Fragile X mental retardation protein targets G quartet mRNAs important for neuronal function. *Cell* 2001; **107**: 489–499.

39. Daigle, J. G. *et al.* RNA-binding ability of FUS regulates neurodegeneration, cytoplasmic mislocalization and incorporation into stress granules associated with FUS carrying ALS-linked mutations. *Hum Mol Genet* 2013; **22**: 1193–1205.

40. Perrone-Bizzozero NI, Tanner DC, Mounce J, Bolognani, F. Increased expression of axogenesis-related genes and mossy fibre length in dentate granule cells from adult HuD overexpressor mice. *ASN Neuro* 2011; **3**: 259–270.

41. Akten B, Kye MJ, Hao LT, Wertz MH, Singh S, Nie D *et al.* Interaction of survival of motor neuron (SMN) and HuD proteins with mRNA cpg15 rescues motor neuron axonal deficits. *Proc Natl Acad Sci USA* 2011; **108**: 10337–10342.

42. Mobarak CD, Anderson KD, Morin M, Beckel-Mitchener A, Rogers SL, Furneaux H *et al.* The RNA-binding protein HuD is required for GAP-43 mRNA stability, GAP-43 gene expression, and PKC-dependent neurite outgrowth in PC12 cells. *Mol Biol Cell* 2000; **11**: 3191–3203.

43. Beckel-Mitchener AC, Miera A, Keller R, Perrone-Bizzozero NI. Poly(A) tail length-dependent stabilization of GAP-43 mRNA by the RNA-binding protein HuD. *J Biol Chem* 2002; **277**: 27996–28002.

44. Yoo S, Kim HH, Kim P, Donnelly CJ, Kalinski AL, Vuppalanchi D *et al.* A HuD-ZBP1 ribonucleoprotein complex localizes GAP-43 mRNA into axons through its 3' untranslated region AU-rich regulatory element. *Journal of neurochemistry* 2013; **126**: 792–804.

45. Marrone L, Poser I, Casci I, Japtok J, Reinhardt P, Janosch A *et al.* Isogenic FUS-eGFP iPSC Reporter Lines Enable Quantification of FUS Stress Granule Pathology that Is Rescued by Drugs Inducing Autophagy. *Stem Cell Reports* 2018; **10**: 375–389.

46. Rohm M, May C, Marcus K, Steinbach S, Theis V, Theiss C *et al.* The microRNA miR-375-3p and the Tumor Suppressor NDRG2 are Involved in Sporadic Amyotrophic Lateral Sclerosis. *Cell Physiol Biochem* 2019; **52**: 1412–1426.

47. Bhinge A, Namboori SC, Bithell A, Soldati C, Buckley NJ, Stanton LW. MiR-375 is Essential for Human Spinal Motor Neuron Development and May Be Involved in Motor Neuron Degeneration. *Stem Cells* 2016; **34**: 124–134.

48. Samson, M. L. Evidence for 3' untranslated region-dependent autoregulation of the Drosophila gene encoding the neuronal nuclear RNA-binding protein ELAV. *Genetics* 1998; **150**: 723–733 (1998).

49. Bolognani, F., Contente-Cuomo, T. & Perrone-Bizzozero, N. I. Novel recognition motifs and biological functions of the RNA-binding protein HuD revealed by genome-wide identification of its targets. *Nucleic Acids Res* 2009; **38,** 117–130.

50. Lenzi J, De Santis R, de Turris V, Morlando M, Laneve P, Calvo A *et al.* ALS mutant FUS proteins are recruited into stress granules in induced Pluripotent Stem Cells (iPSCs) derived motoneurons. *Dis Model Mech* 2015; **8**: 755–766.

51. Birsa N, Ule AM, Garone MG, Tsang B, Mattedi F, Chong PA *et al.* FUS-ALS mutants alter FMRP phase separation equilibrium and impair protein translation. *Science Advances. In press*.

52. Bronicki LM, Jasmin BJ. Emerging complexity of the HuD/ELAVl4 gene; implications for neuronal development, function, and dysfunction. *RNA* 2013; **19**: 1019–1037.

53. García-Mauriño SM, Rivero-Rodríguez F, Velázquez-Cruz A, Hernández-Vellisca M, Díaz-Quintana A, la Rosa De MA *et al.* RNA Binding Protein Regulation and Cross-Talk in the Control of AU-rich mRNA Fate. *Front Mol Biosci* 2017; **4**: 1271.

54. Zhang YQ, Bailey AM, Matthies HJ, Renden RB, Smith MA, Speese SD *et al.* Drosophila fragile X-related gene regulates the MAP1B homolog Futsch to control synaptic structure and function. *Cell* 2001; **107**: 591–603.

55. Coyne AN, Yamada SB, Siddegowda BB, Estes PS, Zaepfel BL, Johannesmeyer JS *et al.* Fragile X protein mitigates TDP-43 toxicity by remodeling RNA granules and restoring translation. *Hum Mol Genet* 2015; **24**: 6886–6898.

56. Majumder P, Chu J-F, Chatterjee B, Swamy KBS, Shen C-KJ. Co-regulation of mRNA translation by TDP-43 and Fragile X Syndrome protein FMRP. *Acta Neuropathol* 2016; **132**: 721–738.

57. Aigner L, Arber S, Kapfhammer JP, Laux T, Schneider C, Botteri F *et al.* Overexpression of the neural growth-associated protein GAP-43 induces nerve sprouting in the adult nervous system of transgenic mice. *Cell* 1995; **83**: 269–278.

58. Harding DI, Greensmith L, Mason M, Anderson PN, Vrbová G. Overexpression of GAP-43 induces prolonged sprouting and causes death of adult motoneurons. *Eur J Neurosci* 1999; **11**: 2237–2242.

59. Wang Z-H, Li S-J, Qi Y, Zhao J-J, Liu X-Y, Han Y *et al.* HuD regulates the cpg15 expression via the 3'-UTR and AU-rich element. *Neurochem Res* 2011; **36**: 1027–1036.

60. Gomes C, Lee JS, Gardiner AS, Smith T, Sahoo PK, Patel P, *et al.* Axonal localization of neuritin/CPG15 mRNA is limited by competition for HuD binding. *J Cell Sci* 2017; **130**: 3650–3662.

61. Nedivi E, Hevroni D, Naot D, Israeli D, Citri Y. Numerous candidate plasticity-related genes revealed by differential cDNA cloning. *Nature* 1993; **363**: 718–722.

62. Fujino T, Lee W-CA, Nedivi E. Regulation of cpg15 by signaling pathways that mediate synaptic plasticity. *Mol Cell Neurosci* 2003; **24**: 538–554.

63. Nedivi E, Fieldust S, Theill LE, Hevron D. A set of genes expressed in response to light in the adult cerebral cortex and regulated during development. *Proc Natl Acad Sci USA* 1996; **93**: 2048–2053.

64. Naeve GS, Ramakrishnan M, Kramer R, Hevroni D, Citri Y, Theill LE. Neuritin: a gene induced by neural activity and neurotrophins that promotes neuritogenesis. *Proc Natl Acad Sci USA* 1997; **94**: 2648–2653.

65. Uhlén M, Fagerberg L, Hallström BM, Lindskog C, Oksvold P, Mardinoglu A *et al.* Proteomics. Tissue-based map of the human proteome. *Science* 2015; **347**: 1260419.

66. Nedivi E, Wu GY, Cline HT. Promotion of dendritic growth by CPG15, an activity-induced signaling molecule. *Science* 1998; **281**: 1863–1866.

67. Cantallops I, Haas K, Cline HT. Postsynaptic CPG15 promotes synaptic maturation and presynaptic axon arbor elaboration in vivo. *Nat Neurosci* 2000; **3**: 1004–1011.

68. Merianda TT, Gomes C, Yoo S, Vuppalanchi D, Twiss JL. Axonal localization of neuritin/CPG15 mRNA in neuronal populations through distinct 5' and 3' UTR elements. *J Neurosci* 2013; **33**: 13735–13742.

69. Javaherian A, Cline HT. Coordinated motor neuron axon growth and neuromuscular synaptogenesis are promoted by CPG15 in vivo. *Neuron* 2005; **45**: 505–512.

70. Bandyopadhyay U, Cotney J, Nagy M, Oh S, Leng J, Mahajan M *et al.* RNA-Seq profiling of spinal cord motor neurons from a presymptomatic SOD1 ALS mouse. *PLoS ONE* 2013; **8**: e53575.

71. Nijssen J, Aguila J, Hoogstraaten R, Kee N, Hedlund E. Axon-Seq Decodes the Motor Axon Transcriptome and Its Modulation in Response to ALS. *Stem Cell Reports* 2018; **11**: 1565–1578.

72. Dell'Orco, M. *et al.* HuD regulates SOD1 expression during oxidative stress in differentiated neuroblastoma cells and sporadic ALS motor cortex. *Neurobiology of Disease* 2021; **148**: 105211.

73. Rosa A, Papaioannou MD, Krzyspiak JE, Brivanlou AH. miR-373 is regulated by TGFβ signaling and promotes mesendoderm differentiation in human Embryonic Stem Cells. *Dev Biol* 2014. doi:10.1016/j.ydbio.2014.03.020.

74. Schindelin J, Arganda-Carreras I, Frise E, Kaynig V, Longair M, Pietzsch T *et al.* Fiji: an open-source platform for biological-image analysis. *Nat Methods* 2012; **9**: 676–682.

FIGURE LEGENDS

Figure 1. Increased HuD levels in human and mouse FUS-mutant MNs.

(A,B) HuD protein levels analysis by western blot in FUS^{WT} and FUS^{P525L} hiPSC-derived spinal MNs (A) and Fus-Δ14 mouse model spinal cord (P81) (B). The molecular weight is indicated on the left. The graphs show the average from 3 independent biological replicates, error bars indicate the standard deviation (panel A: Student's t-test, paired, two tails, *$p < 0.05$; panel B: ordinary one-way ANOVA, multiple comparisons, **$p < 0.01$, ns: $p > 0.05$). TUBB3/Tubb3 signal was used for normalization. (C) HuD mRNA analysis by FISH in FUS^{WT} and FUS^{P525L} hiPSC-derived spinal MNs. The graphs show the average count of *HuD* mRNA puncta per cell from 3 independent differentiation experiments, error bars indicate the standard error of the mean (Student's t-test; paired; two tails; ****$p < 0.0001$; ns: $p > 0.05$). (D,E) Combined PURO-PLA (HuD, magenta) and immunostaining (TUBB3, green) analysis in FUS^{WT} and FUS^{P525L} hiPSC-derived spinal MNs (D) and primary MNs from Fus-Δ14 mouse embryos (E12.5-13.5) (E). DAPI (blue) was used for nuclear staining. In panel (D), FUS^{P525L} hiPSC-derived spinal MNs treated with the eukaryotic protein synthesis inhibitor anisomycin (ANISO) were used as negative control of the PURO-PLA. The graphs show the average count of HuD PURO-PLA puncta per cell from 3 independent differentiation experiments (D) and 3 samples (E), error bars indicate the standard error of the mean (panel D: Student's t-test, unpaired, two tails, ****$p < 0.0001$; panel E: ordinary one-way ANOVA, multiple comparisons, ****$p < 0.0001$; ns: $p > 0.05$). Scale bars in panels (C,D,E): 10 μm.

Figure 2. FMRP and FUS^{P525L} compete for HuD 3'UTR binding

(A) Western blot analysis of the FMRP RIP assay. In: input; IgG: control immunoprecipitation with rabbit monoclonal anti-human IgG antibody; IP: samples immunoprecipitated with an anti-FMRP antibody. The molecular weight is indicated on the left. (B) Analysis of *MAP1B* (positive control), *ATP5O* (negative control) and *HuD* mRNA levels by real time qRT-PCR in samples from FUS^{WT}

(top) or FUS^{P525L} (bottom) hiPSC-derived spinal MNs. The graph shows the relative enrichment of the mRNAs pulled down by FMRP, reported as the percentage of input, in IP or control IgG samples, after normalization with an artificial spike RNA. The graphs show the average from 5 independent differentiation experiments and error bars indicate the standard deviation (Student's t-test; unpaired; two tails; *p < 0.05; **p < 0.01). For anti-FMRP IP samples, yellow dots are related to samples immunoprecipitated with the ab17722 antibody and orange dots to samples immunoprecipitated with the f4055 antibody. (C) Schematic representation of the HuD transcript. The 3 regions of the 3'UTR (F1, F2, F3) used for in vitro binding assays are shown. (D) The *in vitro* binding assay was performed by incubating biotinylated transcripts corresponding to *HuD* 3'UTR regions F1, F2 or F3, or a portion of the Renilla luciferase coding sequence used as negative control (Neg. C), with HeLa cytoplasmic extract, followed by pull-down with streptavidin-conjugated beads. Western blot analysis was then performed with anti-FMRP antibody to detect FMRP binding. Anti-GAPDH was used as negative control. Input: 10% of the pull-down input sample. On the right, histogram showing quantification from 3 independent experiments. Values were calculated as fraction of Input (Student's t-test; paired; two tails; **p < 0.01; ns: p > 0.05). (E) The *in vitro* FMRP binding assay was repeated in presence of purified recombinant FUS proteins. F1 and F2 biotinylated transcripts were incubated with HeLa extract and purified RFP-flag-FUS^{P525L} (indicated as P525L) or an RNA-binding deficient mutant derived from RFP-flag-FUS^{P525L} (indicated as P525L 4F-L). Western blot analysis was performed after pull-down with streptavidin-conjugated beads with anti-FMRP, anti-flag or anti-GAPDH antibody. Input: 10% of the pull-down input sample. Bottom: histograms showing quantification from 3 independent experiments. Values were calculated as fraction of Input and normalized to P525L (Student's t-test; paired; two tails; *p < 0.05; **p < 0.01).

Figure 3. FMRP is a post-transcriptional repressor of HuD expression

(A) Analysis of the protein levels of the indicated genes by western blot in $FMRP^{WT}$ and $FMRP^{KO}$ hiPSC-derived spinal MNs. The molecular weight is indicated on the left. The graphs show the average from 3 independent differentiation experiments, error bars indicate the standard deviation (Student's t-test; paired; two tails; *p < 0.05). TUBB3 signal was used for normalization. (B) Analysis of the mRNA levels of the indicated genes by real-time qRT-PCR in $FMRP^{WT}$ and $FMRP^{KO}$ hiPSC-derived spinal MNs. For each experiment, values are shown as relative to the isogenic $FMRP^{WT}$ control, set to a value of 1. The graph shows the average from 3-5 independent differentiation experiments, error bars indicate the standard deviation (Student's t-test; paired; two tails; p values are indicated; ns: p > 0.05). (C) Luciferase assay in HeLa cells expressing RFP, RFP-FUS^{WT} or RFP-FUS^{P525L} and transfected with the Renilla luciferase reporter construct containing the *HuD* 3'UTR (RLuc-HuD 3'UTR) alone (Mock) or in combination with plasmids overexpressing FMRP or eGFP as a control (Student's t-test; paired; two tails; *p < 0.05; ***p < 0.001; ns: p > 0.05). The drawing on the right depicts the competition between mutant FUS and FMRP for HuD 3'UTR binding and its effects on the reporter construct.

Figure 4. Axonal phenotypes in hiPSC-derived spinal MNs

(A) Representative images, generated with the Skeleton plugin of ImageJ, showing axons of FUS^{WT} and FUS^{P525L} human iPSC-derived MNs in the axon chamber of compartmentalized chips. Scale bar: 100 μm. (B) Quantitative analysis of the number of axon branches and branch points in cells shown in (A). The graphs show the average from 3 independent differentiation experiments, error bars indicate the standard error of the mean (Student's t-test; unpaired; two tails; ****p < 0.0001). (C-E) Immunostaining of TUBB3 (green) in FUS^{WT} and FUS^{P525L} hiPSC-derived spinal MNs cultured in compartmentalized chips and allowed to recover for 30 hours after the indicated treatments to induce axotomy in the axon chamber. Scale bar: 50 μm. Graphs on the right show quantitative analysis of axon length from 3 independent differentiation experiments; error bars indicate the standard error of the mean (Student's t-test; unpaired; two tails; ****p < 0.0001).

Figure 5. Axonal phenotypes in primary spinal MNs from Fus-Δ14 mouse models

(A) Representative images, generated with the Skeleton plugin of ImageJ, showing axons of $Fus^{+/+}$, and heterozygous ($Fus^{\Delta 14/+}$) or homozygous ($Fus^{\Delta 14/\Delta 14}$) FUS mutant mouse primary MNs in the axon chamber of compartmentalized chips. Scale bar: 100 μm. (B) Quantitative analysis of the number of axon branches and branch points in cells shown in (A). The graphs show the average from 3 biological replicates, error bars indicate the standard error of the mean (Ordinary one-way ANOVA; multiple comparisons; ****$p < 0.0001$). (C) Immunostaining of Tubb3 (green) in $Fus^{+/+}$, $Fus^{\Delta 14/+}$ and $Fus^{\Delta 14/\Delta 14}$ mouse primary MNs cultured in compartmentalized chips and allowed to recover for 30 hours after trypsin treatment to induce axotomy in the axon chamber. Scale bar: 100 μm.

Figure 6. NRN1 levels are increased in mutant FUS MNs

(A) Analysis of the mRNA levels of the indicated genes by real time qRT-PCR in FUS^{WT}, FUS^{P525L} and FUS^{WT} overexpressing HuD or RFP, as a control, under the SYN1 promoter (FUS^{WT}+HuD and FUS^{WT}+RFP) hiPSC-derived spinal MNs. The graph shows the average from 3 or 4 independent differentiation experiments, error bars indicate the standard deviation (Student's t-test; paired; two tails; *$p < 0.05$; **$p < 0.01$; ***$p < 0.001$; ns: $p > 0.05$). (B) NRN1 mRNA analysis by FISH (red) in FUS^{WT} and FUS^{P525L} hiPSC-derived spinal MNs. DAPI (blue) was used for nuclear staining. Scale bar: 10 μm. Graphs show the average count of HuD mRNA puncta per cell and the puncta intensity from 3 independent differentiation experiments, error bars indicate the standard error of the mean (Student's t-test; unpaired; two tails; ****$p < 0.0001$). (C,D) NRN1 protein levels analysis by western blot in FUS^{WT} and FUS^{P525L} hiPSC-derived spinal MNs (C) and Fus-Δ14 mouse model spinal cord (D). The molecular weight is indicated on the left. The graphs show the average from 3 independent biological replicates, error bars indicate the standard deviation (Ordinary one-way ANOVA; multiple comparisons; *$p < 0.05$). (E) Immunostaining analysis of NRN1 in axons of

FUS^{WT} and FUS^{P525L} hiPSC-derived spinal MNs. The graph shows the NRN1 signal intensity from 4 replicates from 2 differentiation experiments, error bars indicate the standard error of the mean (Student's t-test; unpaired; two tails; ****p < 0.0001).

Figure 7. GAP43 levels are increased in mutant FUS MNs

(A) GAP43 mRNA analysis by FISH (red) in FUS^{WT}, FUS^{P525L} and FUS^{WT} overexpressing HuD under the Syn1 promoter (FUS^{WT}+HuD) hiPSC-derived spinal MNs. The graphs show the average count of HuD mRNA puncta per cell from 3 independent differentiation experiments, error bars indicate the standard error of the mean (Student's t-test; unpaired; two tails; ****p < 0.0001). DAPI (blue) was used for nuclear staining. Scale bar: 10 μm. (B) GAP43 protein levels analysis by western blot in FUS^{WT} and FUS^{P525L} hiPSC-derived spinal MNs. The molecular weight is indicated on the left. The graph shows the average from 3 independent differentiation experiments and error bars indicate the standard deviation (Student's t-test; paired; two tails; *p < 0.05). TUBB3 signal was used for normalization. (C) Gap43 protein level analysis by western blot in mouse primary spinal MNs (P81). The molecular weight is indicated on the left. The graphs show the average from 3 mice and error bars indicate the standard deviation. The differences are not significant for all pairs (ordinary one-way ANOVA; multiple comparisons). Tubb3 signal was used for normalization. (D) Immunostaining analysis in FUS^{WT} and FUS^{P525L} hiPSC-derived spinal MNs growth cones. GAP43 signal is magenta; PHALLOIDIN signal (marking growth cones) is green, TYR-TUBULIN (tyrosinated alpha-tubulin; marking axons) is white. Scale bar: 10 μm. The graph shows the GAP43 signal intensity from 3 differentiation experiments, error bars indicate the standard error of the mean (Student's t-test; paired; two tails; ****p < 0.0001)

Figure 8. NRN1 knockdown rescues the aberrant axon growth phenotype in mutant FUS MNs

(A) Analysis of the mRNA levels of the indicated genes by real time qRT-PCR in untransfected FUS^{WT} and FUS^{P525L} hiPSC-derived spinal MNs and FUS^{P525L} hiPSC-derived spinal MNs transfected

with non-targeting control siRNAs or siRNAs targeting NRN1. The graph shows the average from 3 independent transfection experiments, error bars indicate the standard deviation (Student's t-test; paired; two tails; *p < 0.05; ns: p > 0.05). (B) Representative images, generated with the Skeleton plugin of ImageJ, showing axons of FUS^{P525L} human iPSC-derived MNs, transfected with the indicated siRNA pools, in the axon chamber of compartmentalized chips. Scale bar: 100 μm. (C) Quantitative analysis of the number of axon branches and branch points. Immunostaining of TUBB3 was carried out 5 days after transfection of the indicated siRNA pools in FUS^{P525L} human iPSC-derived MNs cultured in compartmentalized chips. The graphs show the average from 5 independent transfections of non-targeting or NRN1 siRNAs from 3 differentiation experiments, error bars indicate the standard error of the mean (Student's t-test; unpaired; two tails; ****p < 0.0001). (D) Immunostaining of TUBB3 (green) in FUS^{P525L} hiPSC-derived spinal MNs cultured in compartmentalized chips, transfected with non-targeting control siRNAs or siRNAs targeting NRN1, treated with trypsin in the axon chamber to induce axotomy after 24 hours, and allowed to recover for 24 hours. DAPI (blue) was used for nuclear staining. Scale bar: 100 μm. (E) Graph showing quantitative analysis of axon length in MNs treated as in (D) from 7 independent transfections of non-targeting or NRN1 siRNAs from 2 differentiation experiments, error bars indicate the standard error of the mean (Student's t-test; unpaired; two tails; ****p < 0.0001).

Figure 9. Model

The figure depicts a model of the competition between mutant FUS and FMRP for HuD 3'UTR binding. In FUS^{WT} MNs (top), the FUS protein is predominantly localized in the nucleus. In the cytoplasm, FMRP binds HuD 3'UTR repressing its translation. NRN1 mRNAs are destabilized. In FUS^{P525L} MNs, mutant FUS is partially delocalized to the cytoplasm and outcompetes FMRP binding on the HuD 3'UTR. As a consequence, increased HuD protein levels accumulate in FUS mutant MNs. HuD binding to NRN1 and GAP43 3'UTR leads to stabilization of these transcripts and higher protein levels. NRN1 increase underlies the aberrant axonal growth phenotypes.

A

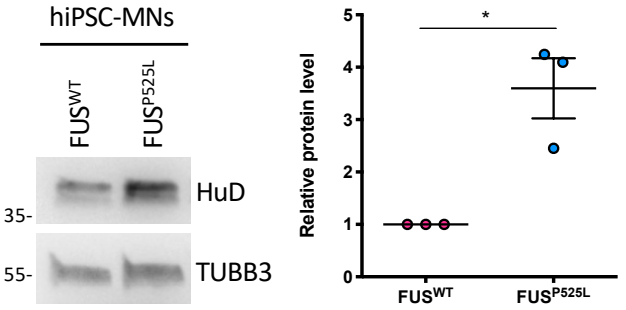

B

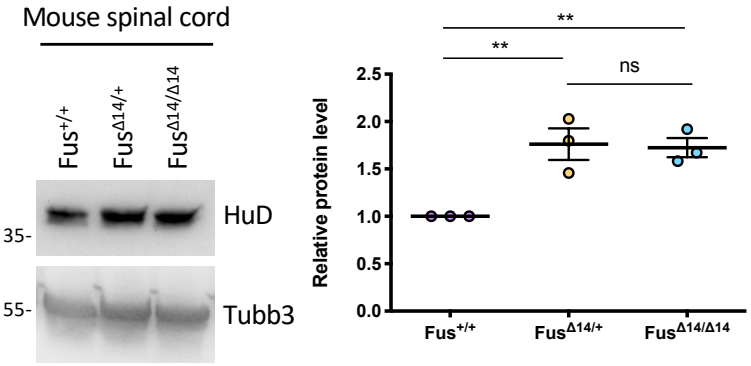

C

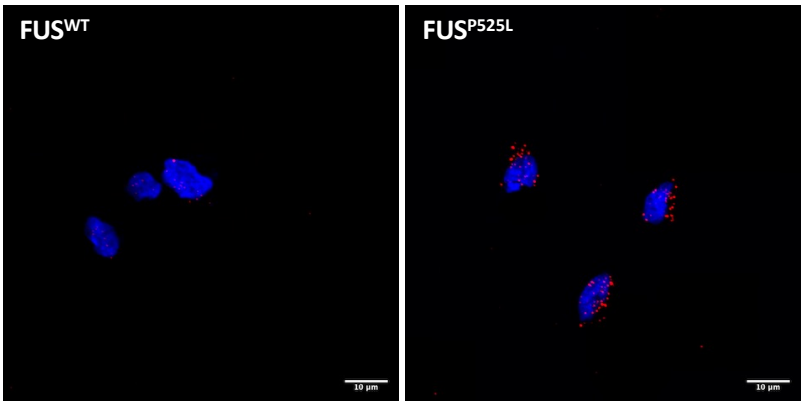

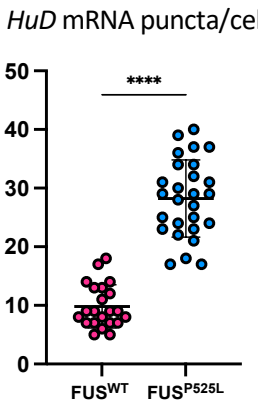

D

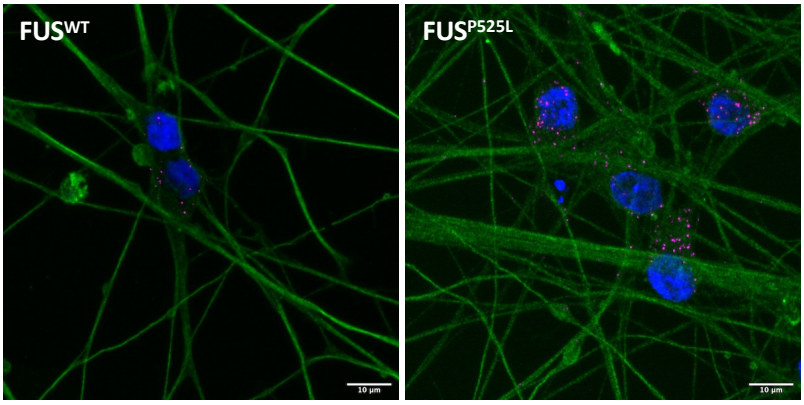

DAPI HuD PURO-PLA TUBB3

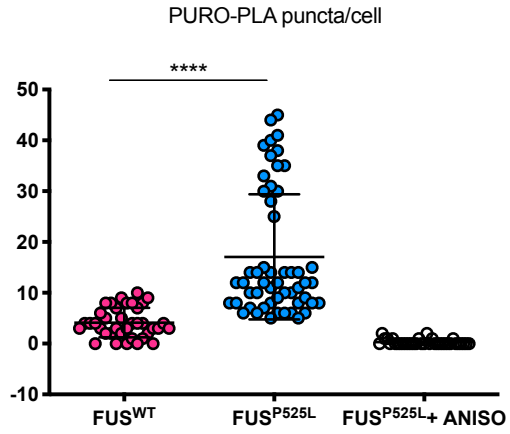

E

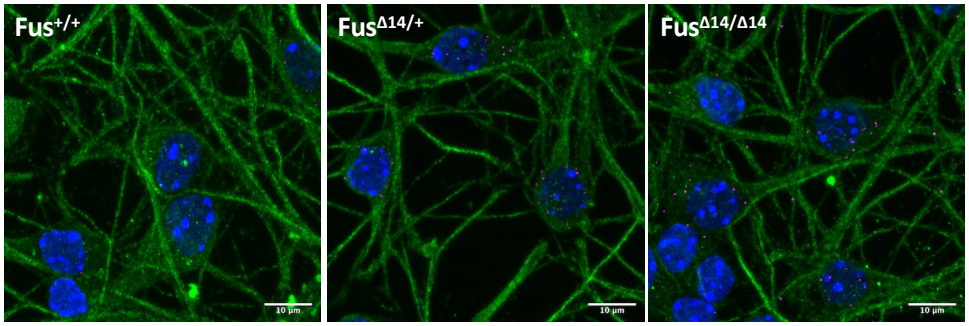

DAPI HuD PURO-PLA Tubb3

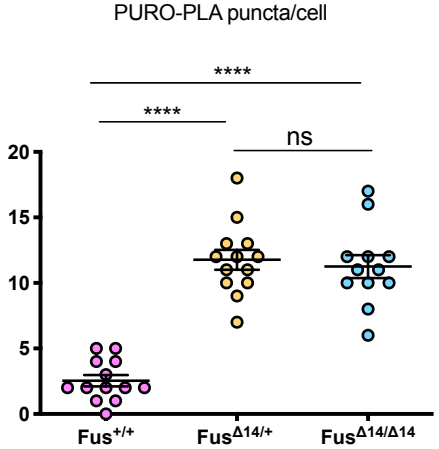

Fig. 2

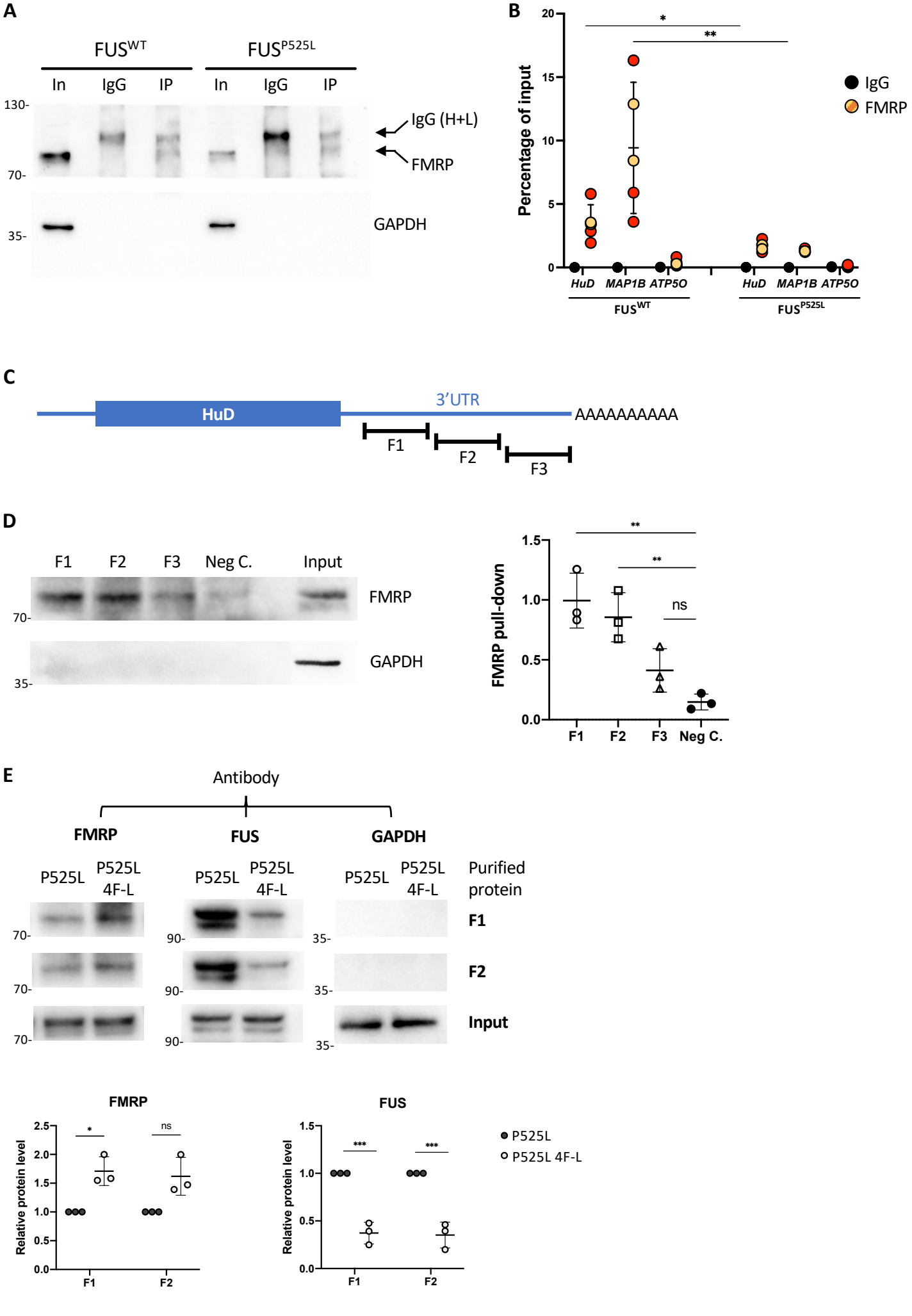

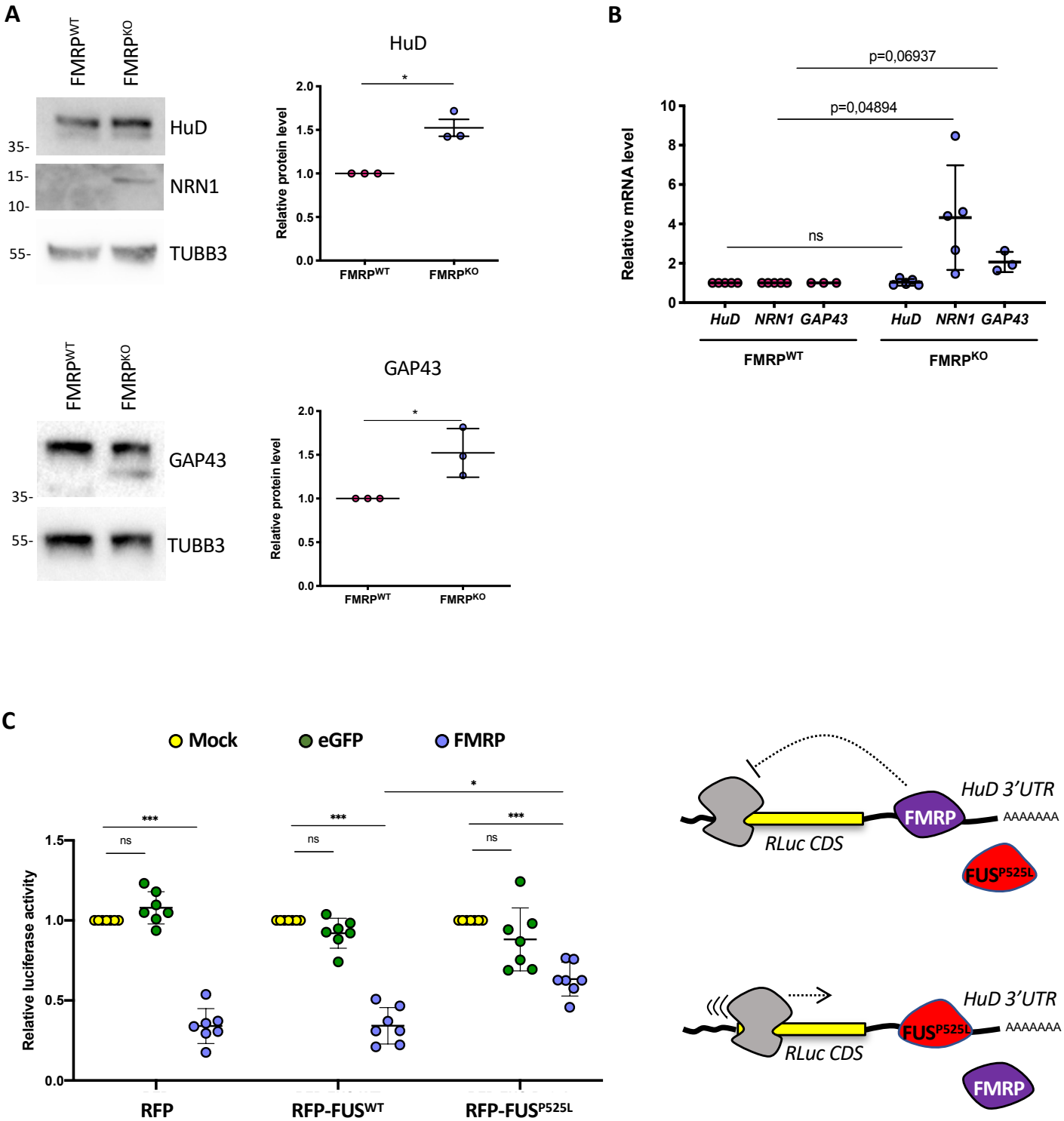

Fig. 4

A

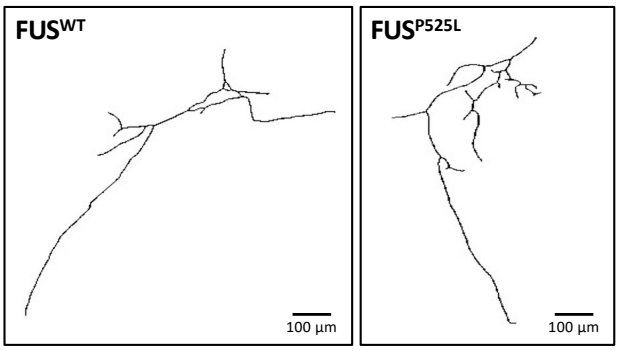

B

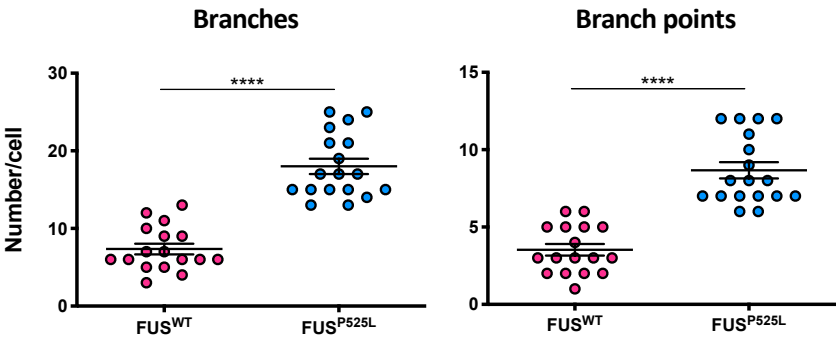

C

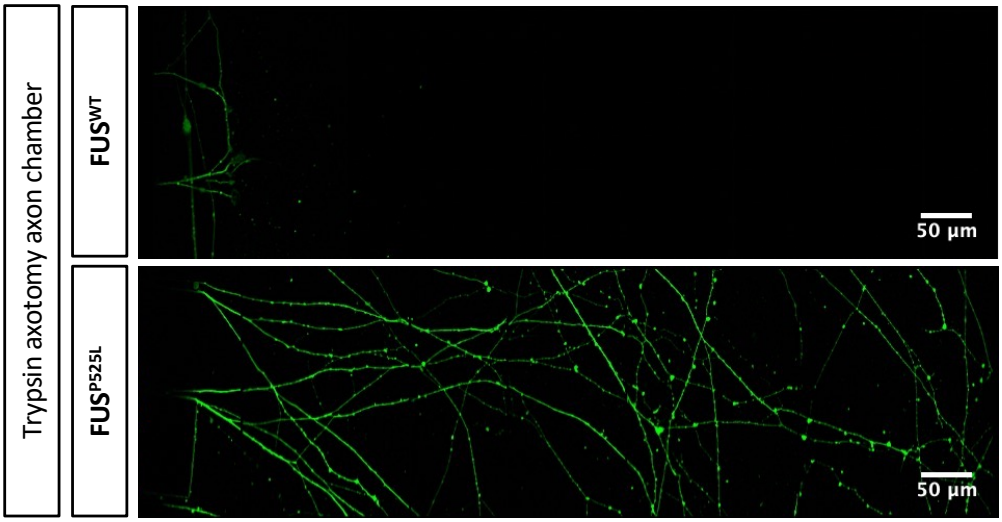

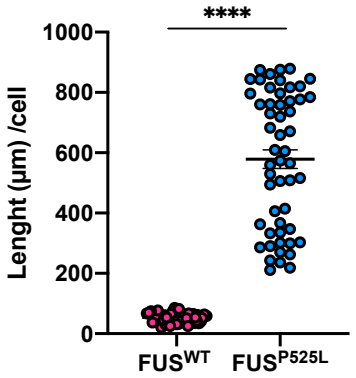

D

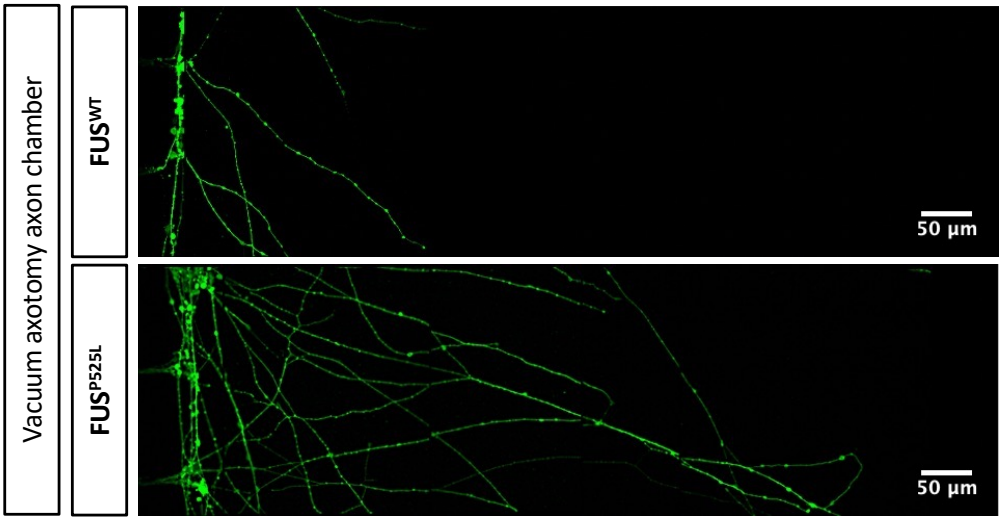

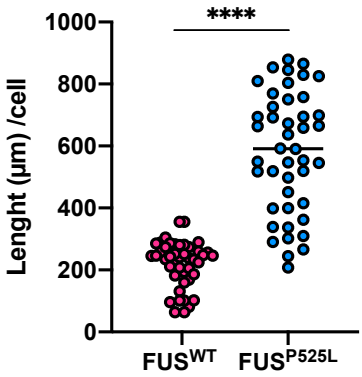

E

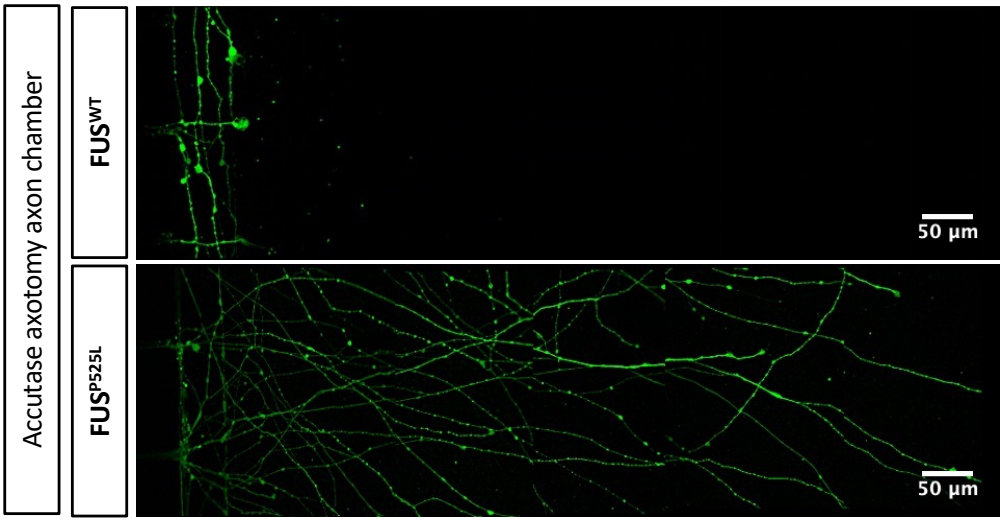

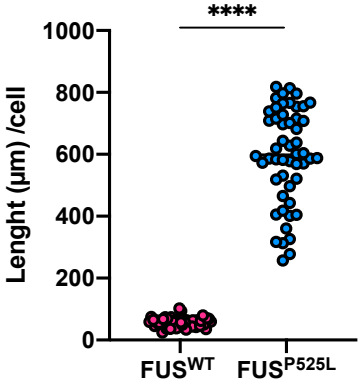

Fig. 5

A

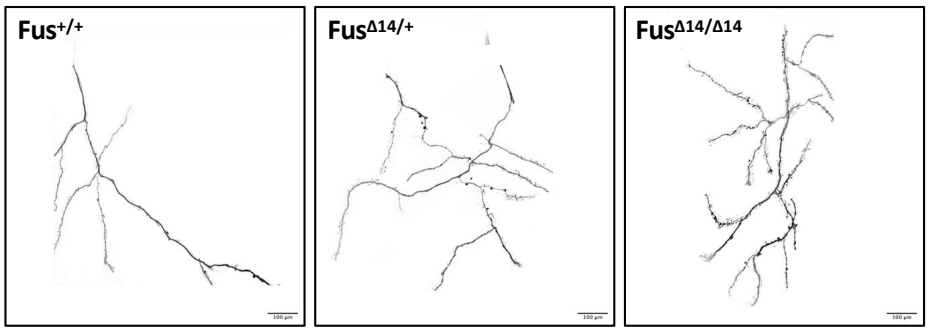

B

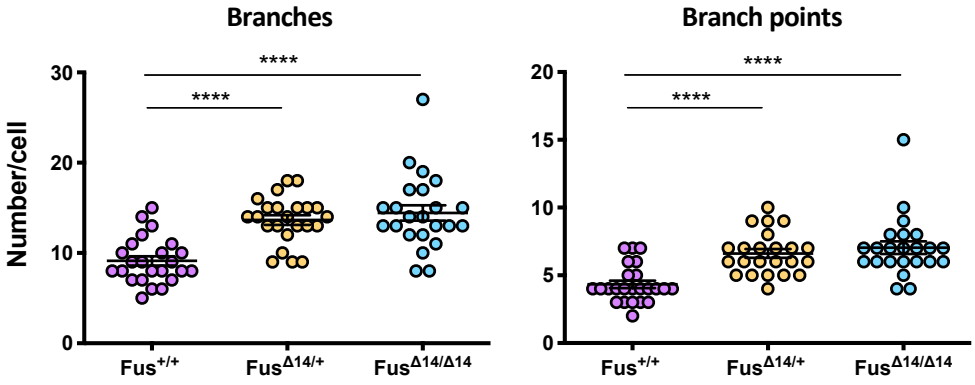

C

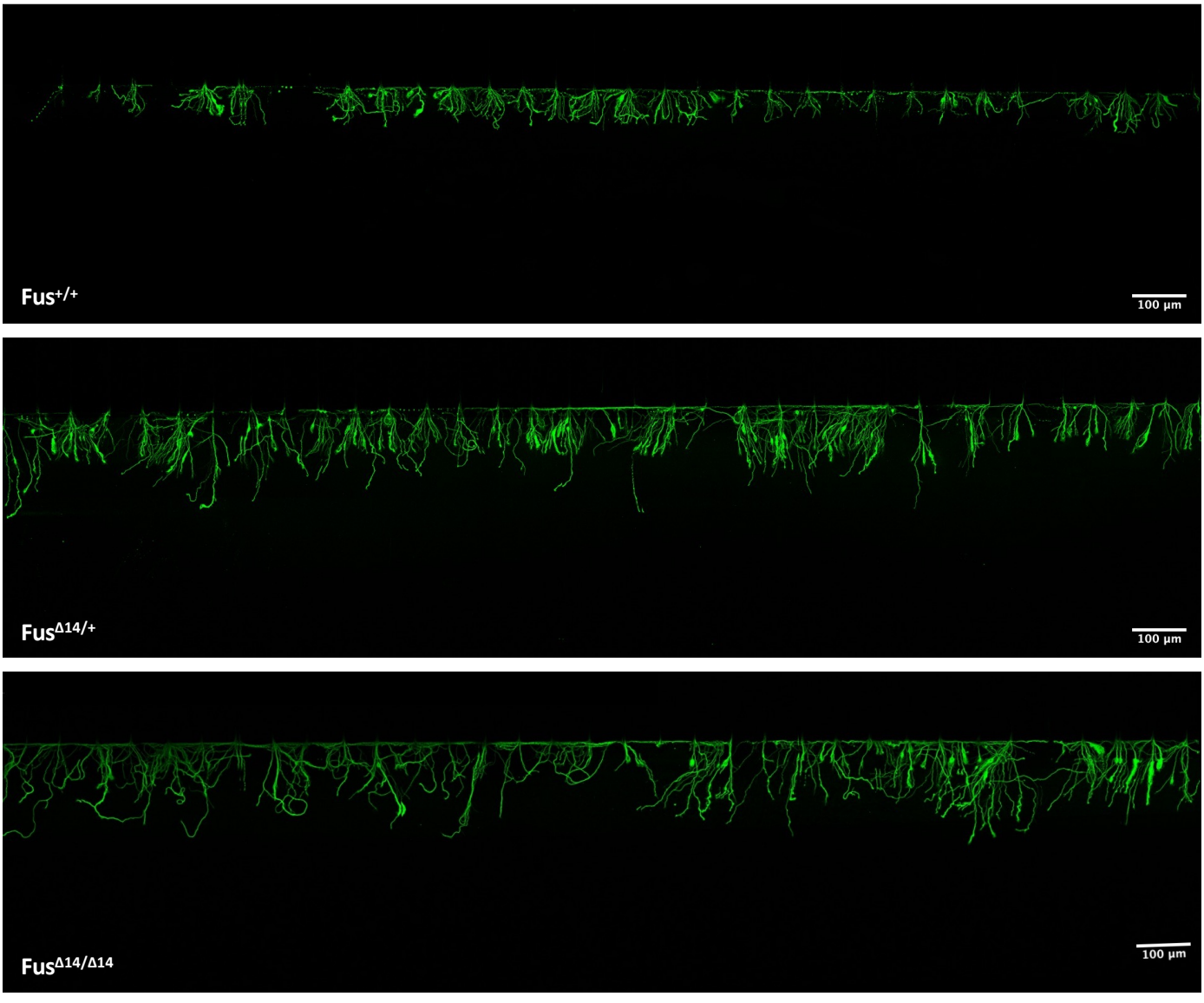

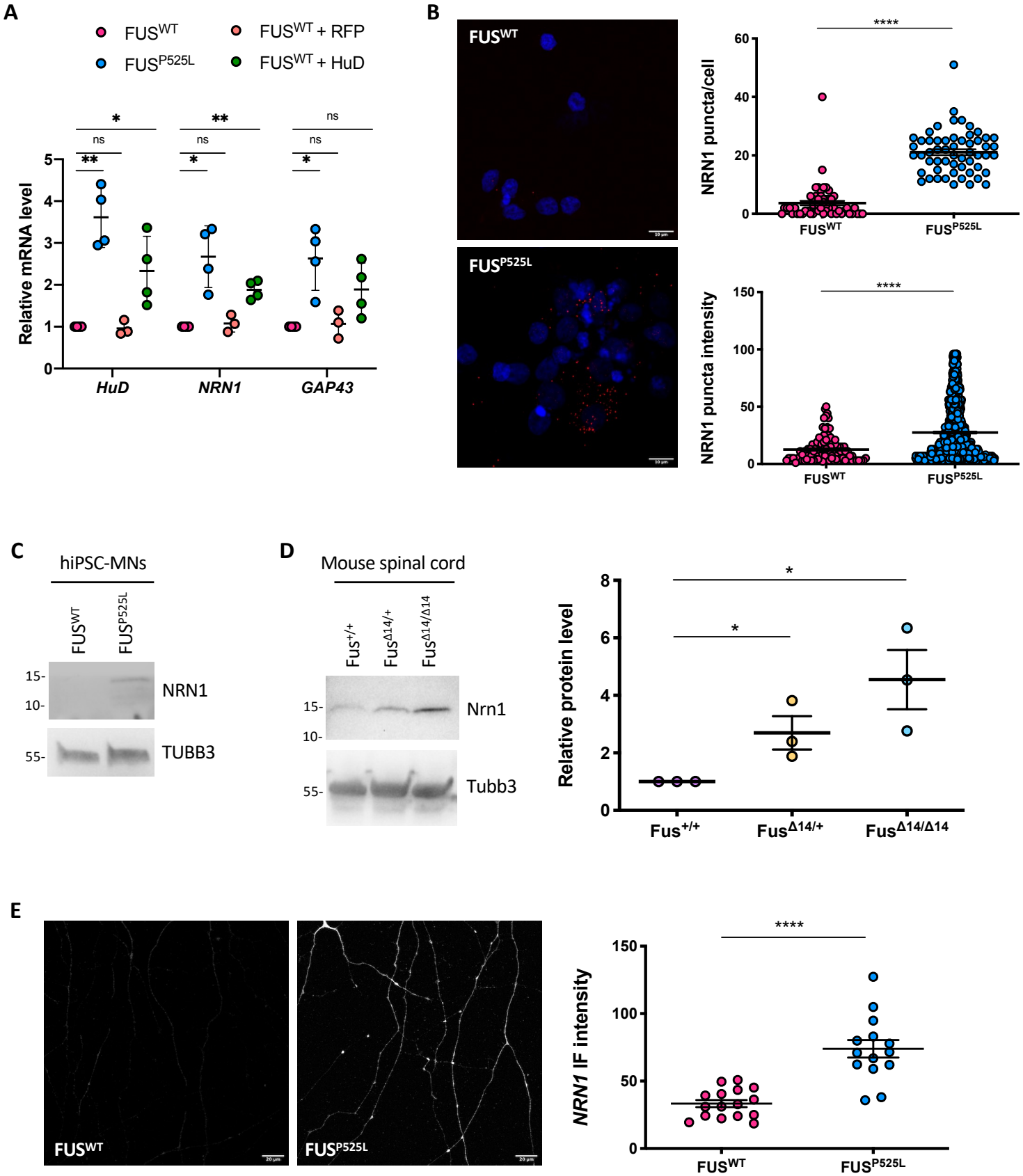

Fig. 7

A

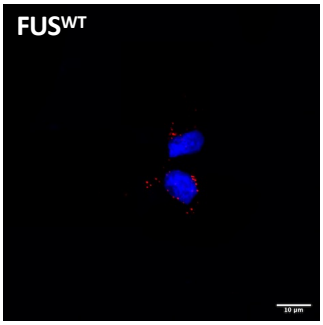

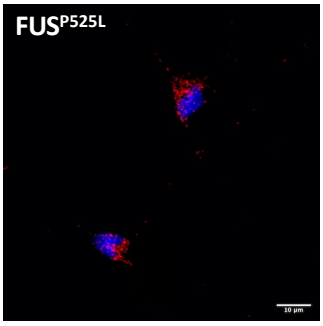

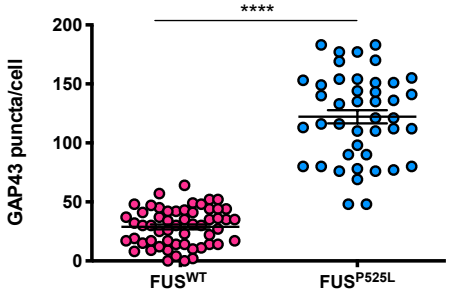

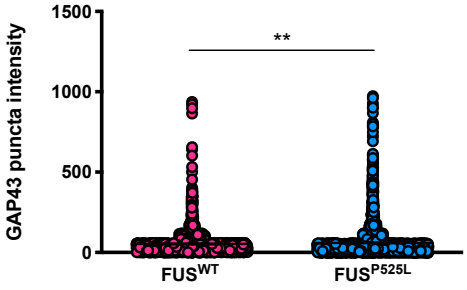

B

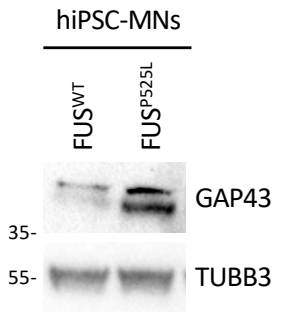

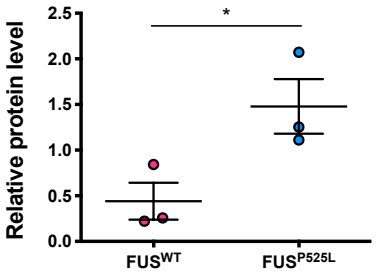

C

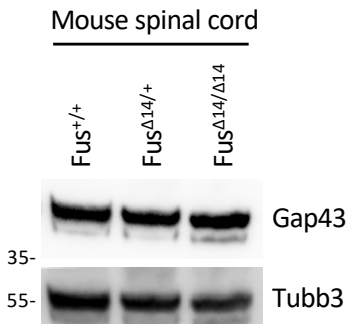

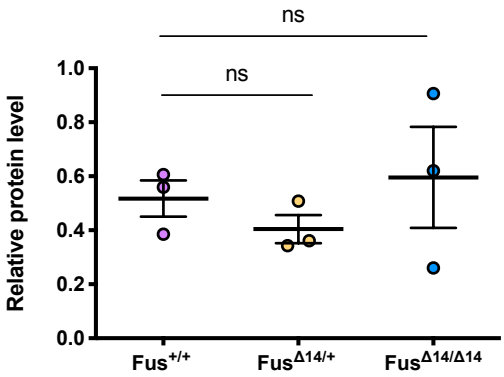

D

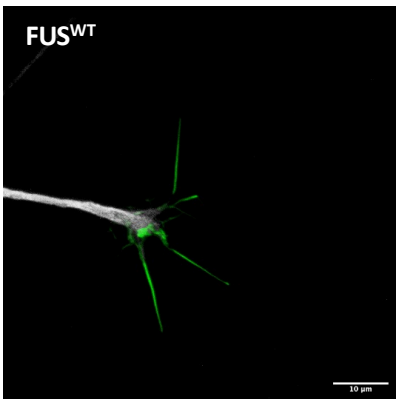

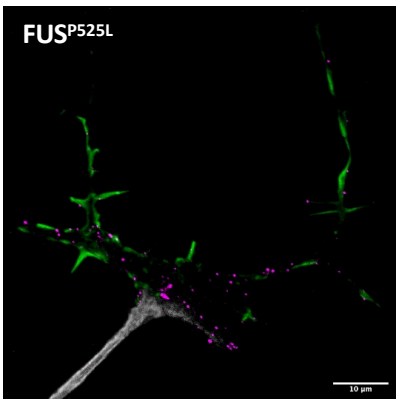

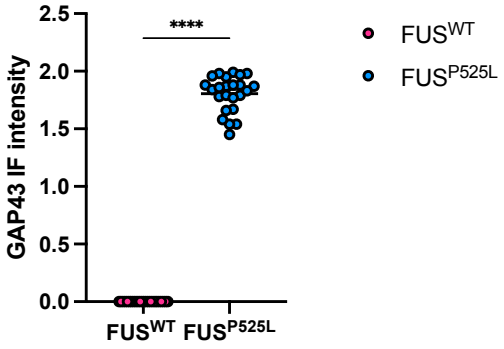

GAP43 PHALLOIDIN TYR-TUBULIN

Fig. 8